## RESEARCH ARTICLE

# Two New and Improved Electronically Adjustable Voltage-Mode Multifunction Biquadratic Filters With Independent Control of Band-Pass, High-Pass, and Low-Pass/Regular Notch Filter Gains

**HUA-PIN CHEN[1], SAN-FU WANG[2], CHIH-YANG CHANG[1], SHIH-JUN CHEN[1], AND YU-HSI CHEN[3]**

[1]Department of Electronic Engineering, Ming Chi University of Technology, Taishan, New Taipei 24301, Taiwan
[2]Department of Electronic Engineering, National Chin-Yi University of Technology, Taiping, Taichung 41170, Taiwan
[3]Department of Electrical Engineering, National Formosa University, Huwei Township, Yunlin 63201, Taiwan

Corresponding author: Hua-Pin Chen (hpchen@mail.mcut.edu.tw)

**ABSTRACT** In this study, two new and improved electronically adjustable voltage-mode (VM) biquadratic filters using three off-the-shelf LT1228 integrated circuits (ICs), two grounded capacitors (GCs), and six resistors are proposed for independent control of the band-pass (BP), high-pass (HP), and low-pass/regular notch (LPN/RN) filter gains. Each proposed electronically adjustable VM multifunction biquadratic filter has one input and six output voltages, enabling simultaneous realization of one low-pass (LP), two BP, two HP, and one LPN/RN filtering responses from the same configuration. Each filter parameter, namely the pole angular frequency ($\omega_o$) and quality factor ($Q$), can be electronically controlled and orthogonally adjusted by the corresponding LT1228 bias current $I_B$. In special cases, the parameters of $\omega_o$ and $Q$ can be electronically controlled and independently adjusted. Each electronically adjustable VM multifunction biquadratic filter has one high input impedance and three low output impedances for independent control of BP, HP, and LPN/RN filter gains. Due to its one high input impedance and three low output impedances, each proposed filter is suitable for cascaded VM circuits without external voltage buffers. Pspice simulations are used to verify the theoretical structure analysis of each proposed LT1228-based electronically adjustable VM multifunction biquadratic filter. Furthermore, experimental tests are performed using three off-the-shelf LT1228 ICs, and several passive components to verify and evaluate the performance of each proposed LT1228-based biquadratic filter.

**INDEX TERMS** LT1228, analog circuit design, integrated circuits, voltage-mode, filters.

## I. INTRODUCTION
High-performance active building blocks (ABBs) are widely used in the design and implementation of analog circuits because they offer wider bandwidth, better signal linearity, greater dynamic range, higher slew-rate, and simpler circuitry than traditional operational amplifiers. For this reason, many analog circuit design techniques using high-performance

The associate editor coordinating the review of this manuscript and approving it for publication was Harikrishnan Ramiah[ID].

ABBs have been published in the open technical literature [1], [2], [3], [4], [5], [6], [7], [8], [9], [10], [11], [12], [13], [14], [15], [16], [17], [18], [19], [20], [21], [22]. VM multifunction biquadratic filters composed of various high-performance ABBs, such as voltage differencing buffered amplifier (VDBA) [23], [24], [25], [26], current feedback amplifier (CFA) [27], [28], [29], [30], [31], [32], differential difference transconductance amplifier (DDTA) [33], voltage differencing differential difference amplifier (VDDDA) [34], voltage differencing differential input buffered

amplifier (VD-DIBA) [35], [36], operational transconductance amplifier (OTA) [37], [38], [39], and LT1228 [40], [41], [42], [43], [44], can be found in the open literature and play an important role in various electronic systems. Biquadratic filters generally implement LP, BP, HP, RN and all-pass (AP) filtering functions, and the other two LPN and HP notch (HPN) filtering functions are special types of RN filtering functions [45], [46]. RN biquadratic filter allows transmission above and below a narrow band by eliminating transmission in a narrow frequency range. The other two special types of notch biquadratic filter are LPN and HPN biquadratic filters [47], [48], [49]. Active biquadratic filters can find many applications in sensor, biomedical, video, and audio crossover network applications [50], [51], [52], [53], [54], [55], [56]. For example, a two-way network divides the bass and high frequency ranges between two speakers [57], while a three-way network divides the bass, midrange and high frequency ranges between three speakers [58], thus requiring the design and implementation of electronically adjustable LP, HP, and BP filters from the same configuration. Moreover, the LPN filter is suitable for electroencephalograph (EEG) applications to eliminate unwanted narrow frequency intervals in the signal [59]. The focus of this study is the simultaneous implementation of LP, BP, HP and LPN/RN filters from the same configuration, providing independent control of their filter gains. Reviewing the technical literature published in [20], [21], [22], [23], [24], [25], [26], [27], [28], [29], [30], [31], [32], [33], [34], [35], [36], [37], [38], [39], [40], [41], [42], and [43], these circuits suffer from one or more of the following drawbacks.

1) Lack of high input impedance for the cascaded input voltage signals [42].
2) Lack of three low output impedances for the cascaded output voltage signals [20], [23], [24], [25], [26], [35], [36], [37], [38], [39], [40], [41], [42].
3) No orthogonal and electronic tunability of the $\omega_o$ and $Q$ [20], [21], [22], [23], [24], [25], [26], [27], [28], [29], [30], [31], [32], [33], [35], [36], [41].
4) No $Q$-value independent and electronic controllability [20], [21], [22], [23], [24], [25], [26], [27], [28], [29], [30], [31], [32], [33], [35], [36], [41].
5) Inability to provide six filtering responses simultaneously in a single topology [20], [21], [22], [23], [24], [25], [26], [27], [28], [29], [30], [31], [32], [33], [35], [36], [37], [38], [39], [40], [41], [42], [43].
6) Inability to provide independent gain control of BP, HP, and LPN/RN filters [20], [21], [22], [23], [24], [25], [26], [27], [28], [29], [30], [31], [32], [33], [34], [35], [36], [37], [38], [39], [40], [41], [42], [43].
7) No experimental verification results for the designed circuit [20], [21], [22], [23], [24], [25], [26].

In particular, studies using commercially available ABBs have attracted the interest of many researchers. Designing a specific circuit using commercially available ABBs is an attractive method to help verify the accuracy and performance of the designed circuit. Consequently, many filter and oscillator implementations have been designed in the open literature and demonstrated using commercially available integrated circuits (ICs), such as the AD844 [2], [6], [7], [8], [9], [12], [27], [28], [29], [30], [31], [32], and [60], LF356 [26], AD830 [34] and [36], AD8130 [35], MAX435 [61] and [62], OPA860 [63], [64] and [65], and CA3080 [26], [66], [67], and [68], LM13600 [69], [70], [71], and LM13700 [16], [33], [34], and [72], and LT1228 [10], [19], [37], [38], [39], [40], [41], [42], [43], [73], [74], [75], [76], and [77]. The commercially available AD844 has a current conveyor followed by an output voltage buffer for driving low impedance loads, but the AD844 does not provide internal electronic capability. To overcome this problem, the commercially available CA3080, LM13600 and LM13700 electronically adjustable OTA active component ICs have been widely used in circuit design. Due to the internal electronic controllability and high output impedance, OTA is suitable for cascading output currents without the need for extra current followers. However, OTA requires additional output voltage buffers for cascading with other VM circuits. LT1228 has received extensive attention as one of the high-performance commercial active components, because it has the characteristics of internal electronic controllability of the pre-stage and low output impedance of the post-stage [40], [41], [42], [43], [44]. Therefore, the LT1228 combines the advantages of an OTA with internal electronic control capability and a CFA with low impedance drive capability. The LT1228 IC uses an external bias control resistor from a series direct current (DC) voltage to adjust the internal bias current ($I_B$) to achieve an electronically adjustable transconductance gain of $g_m$, which is equal to 10 times the value of $I_B$ [19], [43]. Using commercial LT1228 ICs to design a specific circuit is an attractive method to verify the accuracy and efficiency of the designed circuit. In 2021, a single-input and triple-output VM biquadratic filter based on three LT1228 ICs was proposed [42]. However, this circuit does not provide a high-impedance input voltage signal or gain-independent control of the BP, HP, and LPN/RN filter responses. In 2022, two LT1228-based VM multifunction biquadratic filters were recently proposed in [43]. However, each circuit cannot simultaneously provide six filtering responses in a single topology, nor can it achieve independent control of the LPN/RN filtering response gain. Circuits that enable gain-independent controllability of LPN filters can be used for EEG applications [59].

In this paper, two new and improved electronically adjustable VM biquadratic filters are proposed to overcome the above-mentioned drawbacks [20], [21], [22], [23], [24], [25], [26], [27], [28], [29], [30], [31], [32], [33], [34], [35], [36], [37], [38], [39], [40], [41], [42], [43]. Each proposed VM biquadratic filters has one input and six outputs, using three LT1228s, two GCs and six resistors. Using only three commercial LT1228 ICs in each proposed VM biquadratic filter design is very attractive for electronically adjustable filter parameters and driving low-output impedances. It is also attractive to use only two GCs in a VM biquadratic filter

**TABLE 1.** Comparison of the two proposed electronically adjustable filters with the previously validated VM biquadratic filters using off-the-shelf ICs.

| Ref. | No. of Elements Implemented | | Type of Commercial IC Used | (i) | (ii) | (iii) | (iv) | (v) | (vi) | (vii) | (viii) | (ix) |
|---|---|---|---|---|---|---|---|---|---|---|---|---|
| | Device | R + C | | | | | | | | | | |
| [20] | 3 DVCC+ | 2R + 2C | none | LP, BP, HP, RN | no | yes | yes | no | yes | 0 | no | no |
| [21] | 3 DDTA | 0R + 2C | none | LP, 2 BP, HP, RN | no | yes | yes | no | yes | 3 | no | no |
| [22] | 3 CFA | 4R + 2C | 3 AD844 | LP, BP, HP | no | yes | yes | no | yes | 3 | no | no |
| [23] | 2 VDBA | 0R + 2C | none | LP/BP/HP/RN | no | no | yes | no | yes | 1 | no | no |
| [24] | 2 VDBA | 1R + 2C | none | LP/BP/HP/RN/AP | no | no | yes | no | yes | 1 | no | no |
| [25] | 2 VDBA | 0R + 2C | none | LP/BP/HP/RN/AP | no | no | yes | no | yes | 1 | no | no |
| [26] | 2 VDBA | 0R + 2C | CA3080 + LF356 | LP/BP/HP/RN/AP | no | no | yes | no | yes | 1 | no | no |
| [27] | 4 CFA | 4R + 2C | 4 AD844 | LP, BP, HP, RN | no | yes | yes | no | yes | 4 | no | yes |
| [28] | 3 CFA | 3R + 2C | 3 AD844 | LP, BP, RN | no | yes | yes | no | yes | 3 | no | yes |
| [29] | 3 CFA | 4R + 2C | 3 AD844 | LP, BP, RN | no | yes | yes | no | yes | 3 | no | yes |
| [30] | 3 CFA | 4R + 2C | 3 AD844 | LP, BP, HP | no | yes | yes | no | yes | 3 | no | yes |
| [31] | 3 CFA | 3R + 2C | 3 AD844 | LP, BP, RN | no | yes | yes | no | yes | 3 | no | yes |
| [32] | 4 CFA | 5R + 2C | 4 AD844 | LP, BP, HP, RN/AP | no | yes | yes | no | yes | 4 | no | yes |
| [33] | 3 DDTA | 1R + 2C | 6 LM13700 | LP, 2 BP, HP, RN/AP | no | yes | yes | no | yes | 3 | no | yes |
| [34] | 3 VDDDA | 1R+ 2C | 3 LM13700 + 3 AD830 | LP,2 BP, HP, RN, AP | no | yes | yes | no | yes | 3 | yes | yes |
| [35] | 2 VD–DIBA | 2R + 2C | 2 MAX435 + 2 AD8130 | LP, BP, HP | no | yes | yes | no | yes | 1 | no | yes |
| [36] | 2 VD–DIBA | 2R + 2C | 2 LM13700 + 2 AD830 | LP, BP, HP, RN | no | yes | yes | no | yes | 2 | no | yes |
| [37] | 5 OTA | 0R + 2C | 5 LT1228 | LP, BP, RN | no | yes | yes | no | yes | 0 | yes | yes |
| [38] | 5 OTA | 0R + 2C | 5 LT1228 | LP, BP, RN | no | yes | yes | no | yes | 0 | yes | yes |
| [39] | 4 OTA | 0R + 2C | 5 LT1228 | LP, BP, RN | no | yes | yes | no | yes | 0 | yes | yes |
| [40] | 2 LT1228 | 3R + 2C | 2 LT1228 | LP/BP/HP/RN/AP | no | no | yes | no | yes | 1 | no | yes |
| [41] | 3 LT1228 | 3R + 2C | 3 LT1228 | 3 BP | no | yes | yes | no | yes | 2 | yes | yes |
| [42] | 3 LT1228 | 4R + 2C | 3 LT1228 | LP, BP, HP | no | yes | yes | no | no | 2 | no | yes |
| [43] | 3 LT1228 | 5R + 2C | 3 LT1228 | 2 LP,2 BP, HP | no | yes | yes | no | yes | 3 | yes | yes |
| Circuit 1 | 3 LT1228 | 6R + 2C | 3 LT1228 | LP, 2 BP, 2 HP, LPN/RN | yes | yes | yes | yes | yes | 3 | yes | yes |
| Circuit 2 | 3 LT1228 | 6R + 2C | 3 LT1228 | LP, 2 BP, 2 HP, LPN/RN | yes | yes | yes | yes | yes | 3 | yes | yes |

design because the GCs can absorb the equivalent parallel parasitic capacitances. Simultaneous realization of different filter responses from the same configuration will improve its availability, flexibility and cost effectiveness. Both proposed VM LT1228-based circuits offer the following advantages:

(i) They can simultaneously generate LP, BP, HP and LPN/RN filter transfer functions from the same configuration.

(ii) They can implement the LPN transfer function, making it suitable for applications in EEG.

(iii) They only use GCs capable of absorbing parasitic impedances.

(iv) They do not require passive matching conditions to implement any filter transfer functions.

(v) They have independent gain controllability for the BP, HP and LPN/RN filtering responses without affecting the filter parameters of $\omega_o$ and $Q$.

(vi) High input impedance allows cascading with VM circuits at the input.

(vii) The number of low output impedance nodes allows for cascading with VM circuits.

(viii) The parameters $\omega_o$ and $Q$ of the two filters can be electronically and orthogonally/independently adjusted by each corresponding LT1228 of the DC $I_B$.

(iX) The results of the filtering response are verified by computer simulations and hardware experiments.

Based on the use of three off-the-shelf LT1228 ICs in [42] and [43], both proposed circuits can simultaneously generate one LP, two BP, two HP and one LPN/RN filtering responses from the same configuration, and can provide independent gain controllability for the BP, HP and LPN/RN filtering responses without affecting the filter parameters of $\omega_o$ and $Q$. Table 1 shows the comparative characteristics of the two proposed electronically adjustable filters with the previously validated VM biquadratic filters using off-the-shelf ICs. In Table 1, both proposed circuits satisfy all the main advantages compared to the literature studies [20], [21], [22], [23], [24], [25], [26], [27], [28], [29], [30], [31], [32], [33], [34], [35], [36], [37], [38], [39], [40], [41], [42], [43]. Table 2 shows the performance of the two proposed electronically adjustable LT1228-based VM multifunction biquadratic filters compared to the previous VM biquadratic filters [20], [21], [22], [23], [24], [25], [26], [27], [28], [29], [30], [31], [32], [33], [34], [35], [36], [37], [38], [39], [40], [41], [42], [43]. To the best of the authors' knowledge, none of the VM biquadratic filter circuits in [20], [21], [22], [23], [24], [25], [26], [27], [28], [29], [30], [31], [32], [33], [34], [35], [36], [37], [38], [39], [40], [41], [42], and [43] provide

**TABLE 2.** Performance comparison of the two proposed electronically adjustable VM multifunction biquadratic filters with previous VM biquadratic filters.
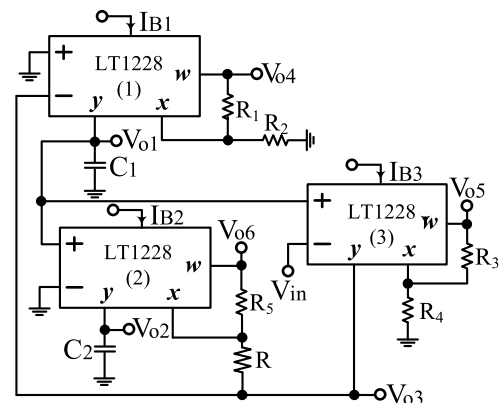
| Ref. | Power supply (V) | Power dissipation (W) | THD (%) | DR (dBc) | IMD3 (dBc) | Phase noise (dBc/Hz) | P1dB (dBm) | FOM (nJ)* | Technology | Obtained results |
|---|---|---|---|---|---|---|---|---|---|---|
| [20] | ±0.75 | $4.36\times10^{-3}$ | 1 @ 200m $V_{pp}$ | 48 | none | none | none | none | 0.13 μm | Simulation |
| [21] | ±0.25 | $0.616\times10^{-6}$ | 0.62 @ 100m $V_{pp}$ | 49.7 | none | none | none | 24.39 | 0.18 μm | Simulation |
| [22] | ±12 | none | none | none | none | none | none | none | AD844 | Simulation |
| [23] | ±0.3 | $7.23\times10^{-6}$ | none | none | none | none | none | none | 0.35 μm | Simulation |
| [24] | ±1.5 | $0.97\times10^{-3}$ | <1 @ 400m $V_{pp}$ | none | none | none | none | none | 0.35 μm | Simulation |
| [25] | ±0.75 | $0.72\times10^{-3}$ | 2 @ 100m $V_{pp}$ | none | none | none | none | none | 0.25 μm | Simulation |
| [26] | ±5 | none | 1.09 @ 100m $V_{pp}$ | 39.37 | none | none | none | none | CA3080 + LF356 | Measured |
| [27] | none | none | none | none | none | none | none | none | AD844 | Measured |
| [28] | ±6 | 0.18 | 0.6 @ 2 $V_{pp}$ | 38.87 | −31.08 | none | 12 | 59.14 | AD844 | Measured |
| [29] | ±6 | 0.16 | none | none | −48.54 | none | 22 | none | AD844 | Measured |
| [30] | ±0.9 | $5.4\times10^{-3}$ | 3.18 @ 1.2 $V_{pp}$ | none | −55.29 | −99.76 @ 1kHz offset | 6 | none | 0.18 μm | Measured |
| [31] | ±6 | 0.25 | none | none | −56.45 | none | 18.8 | none | AD844 | Measured |
| [32] | ±10 | none | none | none | none | none | none | none | AD844 | Measured |
| [33] | 0.5 | $0.83\times10^{-6}$ | 1 @ 80m $V_{pp}$ | 53.27 | none | none | none | $33.66\times10^{-3}$ | 0.13 μm | Simulation |
| [34] | ±5 | 0.34 | <1 @ 650m $V_{pp}$ | none | none | none | none | none | 0.18 μm | Simulation |
| [35] | ±5 | none | 0.5 @ 1.07 $V_{pp}$ | none | none | none | none | none | MAX435 + AD8130 | Measured |
| [36] | ±0.9 | none | 2 @ 400m $V_{pp}$ | none | none | none | none | none | 0.18 μm | Simulation |
| [37] | ±15 | 1.2 | 1.93 @ 200m $V_{pp}$ | none | none | none | none | none | LT1228 | Measured |
| [38] | ±2 ~ ±15 | 0.11 ~ 0.86 | 2 @ 200m $V_{pp}$ | none | −42.35 | none | −14.6 ~ −9.2 | none | LT1228 | Measured |
| [39] | ±15 | 1.23 | 2.13 @ 120m $V_{pp}$ | none | −48.86 | none | −5.9 | none | LT1228 | Measured |
| [40] | ±5 | none | <1.0 @ 180m $V_{pp}$ | none | none | none | none | none | LT1228 | Measured |
| [41] | ±5 | 0.22 | 1.12 @ 120m $V_{pp}$ | 40.86 | −39.66 | −73.87 @ 30Hz offset | −9.7 | none | LT1228 | Measured |
| [42] | ±5 | none | <1 @ 100m $V_{pp}$ | none | none | none | none | none | LT1228 | Measured |
| [43] | ±15 | 0.69 | 0.6 @ 180m $V_{pp}$ | 45.02 | −48.84 | none | −7.1 | 48.74 | LT1228 | Measured |
| Circuit 1 | ±15 | 1.11 | 1 @ 192m $V_{pp}$ | 40.09 | −47.59 | −100.36 @ 1kHz offset | −7.1 | 45.6 | LT1228 | Measured |
| Circuit 2 | ±15 | 0.87 | 1 @ 205m $V_{pp}$ | 40.5 | −46.86 | −100.92 @ 1kHz offset | −7 | 29.37 | LT1228 | Measured |

*FOM = (Power dissipation)/(Order of filter × $f_o$ × DR) [33]
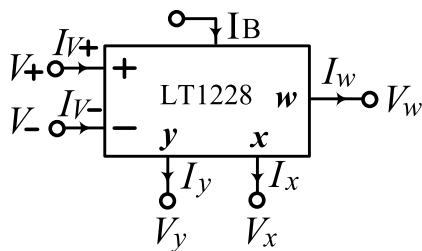


**FIGURE 1.** Circuit symbol of the LT1228.



**FIGURE 2.** First proposed VM biquadratic circuit.

independent gain control for BP, HP, and LPN/RN filter responses without affecting the filter parameters of $\omega_o$ and $Q$. Compared to the VM LT1228-based circuits recently proposed in [42] and [43], these circuits also use the same three LT1228 active components, two GCs and several resistors. From the point of view of today's IC design technology, the use of floating resistors will not cause much impact on the design of ICs. Furthermore, the two proposed electronically adjustable filters can simultaneously generate one LP, two BP, two HP and one LPN/RN filtering responses from the same configuration, and can provide independent gain controllability for the BP, HP and LPN/RN filtering responses.

## II. CIRCUIT DESIGN OF TWO PROPOSED ELECTRONICALLY ADJUSTABLE VM LT1228-BASED MULTIFUNCTION BIQUADRATIC FILTERS

### A. PROPOSED THE FIRST VM MULTIFUNCTION BIQUADRATIC FILTER BASED ON LT1228

The circuit symbol of the LT1228 is shown in Fig. 1. The port characteristics of the LT1228 can be described as

$I_{V+} = I_{V-} = 0$, $I_y = g_m(V_+ - V_-)$, $V_x = V_y$ and $V_w = R_T I_x$, where $g_m$ is the transconductance of the LT1228 and the value of $g_m$ is $10I_B$. $R_T$ is the transresistance gain and the value of $R_T$ is close to infinity [40], [41], [42], [43], [44]. The first proposed electronically adjustable VM multifunction biquadratic filter based on LT1228s is shown in Fig. 2. In Fig. 2, three LT1228s, two GCs and six resistors are used in the design of the first proposed VM multifunction biquadratic circuit. Notably, a single input voltage is connected to the high-input of the third LT1228 negative port, which allows easy cascading of voltage circuits without the use of input voltage buffers. Two GCs are connected to each y terminal of the two LT1228s to absorb the parallel parasitic capacitance. The three output voltages of $V_{o4}$, $V_{o5}$ and $V_{o6}$ are connected to each $w$ terminal of the three LT1228s, which allows easy cascading of voltage circuits without the use of output voltage buffers.

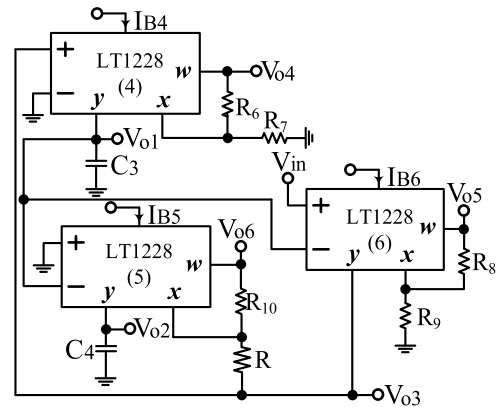Derived from the equations for each node of the first proposed LT1228-based electronically adjustable filter, the nodal analysis equation matrix can be expressed as follows:

$$\begin{bmatrix} sC_1 & 0 & g_{m1} & 0 & 0 & 0 \\ -g_{m2} & sC_2 & 0 & 0 & 0 & 0 \\ -g_{m3} & -\frac{1}{R} & \frac{1}{R} & 0 & 0 & 0 \\ -(1+\frac{R_1}{R_2}) & 0 & 0 & 1 & 0 & 0 \\ 0 & 0 & -(1+\frac{R_3}{R_4}) & 0 & 1 & 0 \\ 0 & -(1+\frac{R_5}{R}) & \frac{R_5}{R} & 0 & 0 & 1 \end{bmatrix} \begin{bmatrix} V_{o1} \\ V_{o2} \\ V_{o3} \\ V_{o4} \\ V_{o5} \\ V_{o6} \end{bmatrix}$$

$$= \begin{bmatrix} 0 \\ 0 \\ -g_{m3}V_{in} \\ 0 \\ 0 \\ 0 \end{bmatrix} \quad (1)$$

Based on Fig. 2, the first proposed LT1228-based electronically adjustable filter has a single input voltage of $V_{in}$, and six output voltages of $V_{o1}$, $V_{o2}$, $V_{o3}$, $V_{o4}$, $V_{o5}$ and $V_{o6}$. According to (1), the following six voltage transfer functions and their filter passband gains can be simultaneously obtained as:

$$\frac{V_{o1}}{V_{in}} = \frac{s\frac{g_{m1}g_{m3}R}{C_1}}{s^2 + s\frac{g_{m1}g_{m3}R}{C_1} + \frac{g_{m1}g_{m2}}{C_1C_2}}, \quad Ho1 = 1 \quad (2)$$

$$\frac{V_{o2}}{V_{in}} = \frac{g_{m3}R(\frac{g_{m1}g_{m2}}{C_1C_2})}{s^2 + s\frac{g_{m1}g_{m3}R}{C_1} + \frac{g_{m1}g_{m2}}{C_1C_2}}, \quad Ho2 = g_{m3}R \quad (3)$$

$$\frac{V_{o3}}{V_{in}} = \frac{-g_{m3}Rs^2}{s^2 + s\frac{g_{m1}g_{m3}R}{C_1} + \frac{g_{m1}g_{m2}}{C_1C_2}}, \quad Ho3 = g_{m3}R \quad (4)$$

$$\frac{V_{o4}}{V_{in}} = \frac{(1+\frac{R_1}{R_2})(s\frac{g_{m1}g_{m3}R}{C_1})}{s^2 + s\frac{g_{m1}g_{m3}R}{C_1} + \frac{g_{m1}g_{m2}}{C_1C_2}}, \quad Ho4 = 1 + \frac{R_1}{R_2} \quad (5)$$

$$\frac{V_{o5}}{V_{in}} = \frac{-g_{m3}R(1+\frac{R_3}{R_4})s^2}{s^2 + s\frac{g_{m1}g_{m3}R}{C_1} + \frac{g_{m1}g_{m2}}{C_1C_2}}, \quad Ho5 = g_{m3}R(1+\frac{R_3}{R_4}) \quad (6)$$

$$\frac{V_{o6}}{V_{in}} = \frac{g_{m3}R_5[s^2 + (1+\frac{R}{R_5})(\frac{g_{m1}g_{m2}}{C_1C_2})]}{s^2 + s\frac{g_{m1}g_{m3}R}{C_1} + \frac{g_{m1}g_{m2}}{C_1C_2}} \quad (7)$$

In (7), the high frequency gain and low frequency gain of the LPN are $g_{m3}R_5$ and $g_{m3}R_5(1 + R/R_5)$, respectively. Letting $R_5 \gg R$ (i.e. $R_5 = 10R$), (7) becomes

$$\frac{V_{o6}}{V_{in}} \approx \frac{g_{m3}R_5(s^2 + \frac{g_{m1}g_{m2}}{C_1C_2})}{s^2 + s\frac{g_{m1}g_{m3}R}{C_1} + \frac{g_{m1}g_{m2}}{C_1C_2}}, \quad Ho6 = g_{m3}R_5 \quad (8)$$

Therefore, the non-inverting RN voltage transfer function with $g_{m3}R_5$ gain is implemented by (8).

Based on (2) to (8), a non-inverting BP voltage transfer function with unity gain is implemented from $V_{o1}$, a non-inverting LP voltage transfer function with $g_{m3}R$ gain is implemented from $V_{o2}$, an inverting HP voltage transfer function with $g_{m3}R$ gain is implemented from $V_{o3}$, a non-inverting BP voltage transfer function with $(1 + R_1/R_2)$ gain is implemented from $V_{o4}$, an inverting HP voltage transfer function with $g_{m3}R(1 + R_3/R_4)$ gain is implemented from $V_{o5}$, and a non-inverting LPN voltage function with $g_{m3}R_5$ (high frequency gain) and $g_{m3}R_5(1 + R/R_5)$ (low frequency gain) is implemented from $V_{o6}$, or a non-inverting RN voltage transfer function with $g_{m3}R_5$ gain is implemented from $V_{o6}$. Note that resistors $R_1$, $R_2$, $R_3$, $R_4$ and $R_5$ can control their filtering gain independently. Table 3 summarizes the parameters of the first proposed electronically adjustable filter. As shown in Table 3, the $Q$-factor can be controlled electronically and independently without affecting the pole frequency $f_o$ of the first proposed filter, and the passband gains of $V_{o4}$, $V_{o5}$ and $V_{o6}$ can be independently control without affecting the $f_o$ value and $Q$-factor. In addition, the three output voltages of $V_{o4}$, $V_{o5}$ and $V_{o6}$ are each connected to the $w$ terminal of the LT1228, enabling the cascading of the VM filters without the use of voltage buffers.

In Table 3, substituting the bias currents of $10I_{Bi}$ ($i = 1, 2, 3$) into the three transconductance amplifies of $g_{mi}$, the $f_o$ and $Q$ can be rewritten as follows:

$$f_o = \frac{5}{\pi}\sqrt{\frac{I_{B1}I_{B2}}{C_1C_2}} \quad (9)$$

$$Q = \frac{1}{10I_{B3}R}\sqrt{\frac{C_1I_{B2}}{C_2I_{B1}}} \quad (10)$$

The $f_o$ and $Q$ can be electronically controlled by biasing the currents of their corresponding LT1228s in (9) and (10). If the two bias currents of $I_{B1} = I_{B2}$, and the two capacitors of $C_1 = C_2 = C$ are substituted into (9) and (10), then the $f_o$ and $Q$ become

$$f_o = \frac{5I_{B1}}{\pi C}, \text{ and } Q = \frac{1}{10I_{B3}R} \quad (11)$$

**TABLE 3.** Summary of the first proposed LT1228-based filter parameters.

| Filter parameters | Pole frequency of $f_o$ | $f_o = \dfrac{1}{2\pi}\sqrt{\dfrac{g_{m1}g_{m2}}{C_1 C_2}}$ |
|---|---|---|
| | Quality factor of $Q$ | $Q = \dfrac{1}{g_{m3}R}\sqrt{\dfrac{C_1 g_{m2}}{C_2 g_{m1}}}$ |
| Filter passband gains | BP gain at $V_{o1}$ | $H_{o1} = 1$ |
| | LP gain at $V_{o2}$ | $H_{o2} = g_{m3}R$ |
| | HP gain at $V_{o3}$ | $H_{o3} = g_{m3}R$ |
| | BP gain at $V_{o4}$ | $H_{o4} = 1 + \dfrac{R_1}{R_2}$ |
| | HP gain at $V_{o5}$ | $H_{o5} = g_{m3}R(1 + \dfrac{R_3}{R_4})$ |
| | LPN gain at $V_{o6}$ | $H_{o6} = g_{m3}R_5$ (high frequency) |
| | | $H_{o6} = g_{m3}R_5(1 + \dfrac{R}{R_5})$ (low frequency) |
| | RN gain at $V_{o6}$ | $H_{o6} = g_{m3}R_5$ |
| Independent gain controllable without affecting $f_o$ and $Q$ | BP gain at $V_{o4}$ | Gain control of $R_1$ or/and $R_2$ |
| | HP gain at $V_{o5}$ | Gain control of $R_3$ or/and $R_4$ |
| | LPN/RN gain at $V_{o6}$ | Gain control of $R_5$ |

In this particular case, the $f_o$ and $Q$ can be controlled electronically and independently by biasing the currents of their corresponding LT1228s.

The LPN has a notch zero frequency $\omega_n$ relative to the pole angular frequency $\omega_o$. In the case of $\omega_n > \omega_o$ in (7), the magnitude response of the LPN can be obtained. According to (7), $\omega_o$ and $\omega_n$ are given by

$$\omega_o = \sqrt{\frac{g_{m1}g_{m2}}{C_1 C_2}} \tag{12}$$

$$\omega_n = \sqrt{(1 + \frac{R}{R_5})(\frac{g_{m1}g_{m2}}{C_1 C_2})} \tag{13}$$

### B. PROPOSED THE SECOND VM FILTER BASED ON LT1228

The second proposed electronically adjustable VM filter based on LT1228s is shown in Fig. 3. In Fig. 3, three LT1228s, two GCs and six resistors are used in the design of the second proposed VM multifunction biquadratic circuit. Notably, a single input voltage is connected to the high-input of the sixth LT1228 positive port, which allows easy cascading of voltage circuits without the use of input voltage buffers. Two GCs are connected to each $y$ terminal of the two LT1228s to absorb the parallel parasitic capacitance. The three output voltages of $V_{o4}$, $V_{o5}$ and $V_{o6}$ are connected to each $w$ terminal of the three LT1228s, which allows easy cascading of voltage circuits without the use of output voltage buffers.

Derived from the equations for each node of the second proposed LT1228-based electronically adjustable filter, the



**FIGURE 3.** Second proposed VM biquadratic circuit.

nodal analysis equation matrix can be expressed as follows:

$$\begin{bmatrix} sC_3 & 0 & -g_{m4} & 0 & 0 & 0 \\ g_{m5} & sC_4 & 0 & 0 & 0 & 0 \\ g_{m6} & -\frac{1}{R} & \frac{1}{R} & 0 & 0 & 0 \\ -(1 + \frac{R_6}{R_7}) & 0 & 0 & 1 & 0 & 0 \\ 0 & 0 & -(1 + \frac{R_8}{R_9}) & 0 & 1 & 0 \\ 0 & -(1 + \frac{R_{10}}{R}) & \frac{R_{10}}{R} & 0 & 0 & 1 \end{bmatrix} \begin{bmatrix} V_{o1} \\ V_{o2} \\ V_{o3} \\ V_{o4} \\ V_{o5} \\ V_{o6} \end{bmatrix}$$
$$= \begin{bmatrix} 0 \\ 0 \\ g_{m6}V_{in} \\ 0 \\ 0 \\ 0 \end{bmatrix} \tag{14}$$

Based on Fig. 3, the second proposed LT1228-based electronically adjustable filter has a single input voltage of $V_{in}$, and six output voltages of $V_{o1}$, $V_{o2}$, $V_{o3}$, $V_{o4}$, $V_{o5}$ and $V_{o6}$. According to (14), the following six voltage transfer functions and their filter passband gains can be simultaneously obtained as:

$$\frac{V_{o1}}{V_{in}} = \frac{s\frac{g_{m4}g_{m6}R}{C_3}}{s^2 + s\frac{g_{m4}g_{m6}R}{C_3} + \frac{g_{m4}g_{m5}}{C_3 C_4}}, \quad H_{o1} = 1 \tag{15}$$

$$\frac{V_{o2}}{V_{in}} = \frac{-g_{m6}R(\frac{g_{m4}g_{m5}}{C_3 C_4})}{s^2 + s\frac{g_{m4}g_{m6}R}{C_3} + \frac{g_{m4}g_{m5}}{C_3 C_4}}, \quad H_{o2} = g_{m6}R \tag{16}$$

$$\frac{V_{o3}}{V_{in}} = \frac{g_{m6}Rs^2}{s^2 + s\frac{g_{m4}g_{m6}R}{C_3} + \frac{g_{m4}g_{m5}}{C_3 C_4}}, \quad H_{o3} = g_{m6}R \tag{17}$$

$$\frac{V_{o4}}{V_{in}} = \frac{(1 + \frac{R_6}{R_7})(s\frac{g_{m4}g_{m6}R}{C_3})}{s^2 + s\frac{g_{m4}g_{m6}R}{C_3} + \frac{g_{m4}g_{m5}}{C_3 C_4}}, \quad H_{o4} = 1 + \frac{R_6}{R_7} \tag{18}$$

$$\frac{V_{o5}}{V_{in}} = \frac{g_{m6}R(1 + \frac{R_8}{R_9})s^2}{s^2 + s\frac{g_{m4}g_{m6}R}{C_3} + \frac{g_{m4}g_{m5}}{C_3 C_4}}, \quad H_{o5} = g_{m6}R(1 + \frac{R_8}{R_9}) \tag{19}$$

$$\frac{V_{o6}}{V_{in}} = \frac{-g_{m6}R_{10}[s^2 + (1 + \frac{R}{R_{10}})(\frac{g_{m4}g_{m5}}{C_3 C_4})]}{s^2 + s\frac{g_{m4}g_{m6}R}{C_3} + \frac{g_{m4}g_{m5}}{C_3 C_4}} \tag{20}$$

In (20), the high frequency gain and low frequency gain of the LPN are $g_{m6}R_{10}$ and $g_{m6}R_{10}(1 + R/R_{10})$, respectively. Letting $R_{10} \gg R$ (i.e. $R_{10} = 10R$), (20) becomes

$$\frac{V_{o6}}{V_{in}} \approx \frac{-g_{m6}R_{10}(s^2 + \frac{g_{m4}g_{m5}}{C_3C_4})}{s^2 + s\frac{g_{m4}g_{m6}R}{C_3} + \frac{g_{m4}g_{m5}}{C_3C_4}}, \quad \text{Ho6} = g_{m6}R_{10} \quad (21)$$

Therefore, the inverting RN voltage transfer function with $g_{m6}R_{10}$ gain is implemented by (21).

Based on (15) to (21), a non-inverting BP voltage transfer function with unity gain is implemented from $V_{o1}$, an inverting LP voltage transfer function with $g_{m6}R$ gain is implemented from $V_{o2}$, a non-inverting HP voltage transfer function with $g_{m6}R$ gain is implemented from $V_{o3}$, a non-inverting BP voltage transfer function with $(1 + R_6/R_7)$ gain is implemented from $V_{o4}$, a non-inverting HP voltage transfer function with $g_{m6}R(1 + R_8/R_9)$ gain is implemented from $V_{o5}$, and an inverting LPN voltage function with $g_{m6}R_{10}$ (high frequency gain) and $g_{m6}R_{10}(1 + R/R_{10})$ (low frequency gain) is implemented from $V_{o6}$, or an inverting RN voltage transfer function with $g_{m6}R_{10}$ gain is implemented from $V_{o6}$. Note that resistors $R_6$, $R_7$, $R_8$, $R_9$ and $R_{10}$ can control their filtering gain independently. Table 4 summarizes the parameters of the second proposed electronically adjustable VM biquadratic filter. As shown in Table 4, the $Q$-factor can be controlled electronically and independently without affecting the pole frequency $f_o$ of the second proposed filter, and the passband gains of $V_{o4}$, $V_{o5}$ and $V_{o6}$ can be independently control without affecting the $f_o$ value and $Q$-factor. In addition, the three output voltages of $V_{o4}$, $V_{o5}$ and $V_{o6}$ are each connected to the $w$ terminal of the LT1228, enabling the cascading of the VM filters without the use of voltage buffers.

In Table 4, substituting the bias currents of $10I_{Bj}$ $(j = 4, 5, 6)$ into the three transconductance amplifies of $g_{mj}$, the $f_o$ and $Q$ can be rewritten as follows:

$$f_o = \frac{5}{\pi}\sqrt{\frac{I_{B4}I_{B5}}{C_3C_4}} \quad (22)$$

$$Q = \frac{1}{10I_{B6}R}\sqrt{\frac{C_3I_{B5}}{C_4I_{B4}}} \quad (23)$$

The $f_o$ and $Q$ can be electronically controlled by biasing the currents of their corresponding LT1228s in (22) and (23). If the two bias currents of $I_{B4} = I_{B5}$, and the two capacitors of $C_3 = C_4 = C$ are substituted into (22) and (23), then the $f_o$ and $Q$ become

$$f_o = \frac{5I_{B4}}{\pi C}, \quad \text{and} \quad Q = \frac{1}{10I_{B6}R} \quad (24)$$

In this particular case, the $f_o$ and $Q$ can be controlled electronically and independently by biasing the currents of their corresponding LT1228s.

In the case of $\omega_n > \omega_o$ in (20), the magnitude response of the LPN can be obtained. According to (20), $\omega_o$ and $\omega_n$ are given by

$$\omega_o = \sqrt{\frac{g_{m4}g_{m5}}{C_3C_4}} \quad (25)$$

**TABLE 4.** Summary of the second proposed LT1228-based filter parameters.

| | | |
|---|---|---|
| Filter parameters | Pole frequency of $f_o$ | $f_o = \frac{1}{2\pi}\sqrt{\frac{g_{m5}g_{m6}}{C_3C_4}}$ |
| | Quality factor of $Q$ | $Q = \frac{1}{g_{m6}R}\sqrt{\frac{C_3g_{m5}}{C_4g_{m4}}}$ |
| Filter passband gains | BP gain at $V_{o1}$ | $H_{o1} = 1$ |
| | LP gain at $V_{o2}$ | $H_{o2} = g_{m6}R$ |
| | HP gain at $V_{o3}$ | $H_{o3} = g_{m6}R$ |
| | BP gain at $V_{o4}$ | $H_{o4} = 1 + \frac{R_6}{R_7}$ |
| | HP gain at $V_{o5}$ | $H_{o5} = g_{m6}R(1 + \frac{R_8}{R_9})$ |
| | LPN gain at $V_{o6}$ | $H_{o6} = g_{m6}R_{10}$ (high frequency) |
| | | $H_{o6} = g_{m6}R_{10}(1 + \frac{R}{R_5})$ (low frequency) |
| | RN gain at $V_{o6}$ | $H_{o6} = g_{m6}R_{10}$ |
| Independent gain controllable without affecting $\omega_o$ and $Q$ | BP gain at $V_{o4}$ | Gain control of $R_6$ or/and $R_7$ |
| | HP gain at $V_{o5}$ | Gain control of $R_8$ or/and $R_9$ |
| | LPN/RN gain at $V_{o6}$ | Gain control of $R_{10}$ |
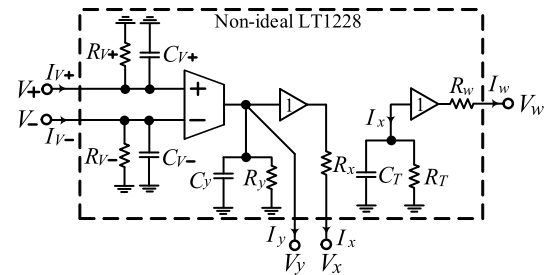
**FIGURE 4.** Circuit symbol of the LT1228.
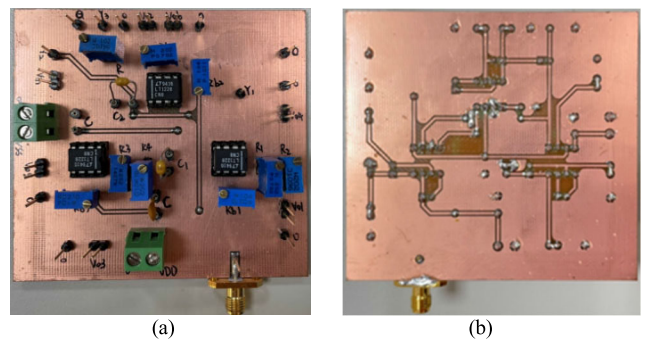
**FIGURE 5.** First PCB prototype (a) top view and (b) bottom view of the measurement circuit in Fig. 2.

$$\omega_n = \sqrt{(1 + \frac{R}{R_{10}})(\frac{g_{m4}g_{m5}}{C_3C_4})} \quad (26)$$

## C. EFFECT OF THE PARASITIC IMPEDANCES OF THE LT1228 ON THE TWO PROPOSED LT1228-BASED CIRCUITS

Figure 4 shows the LT1228 and its parasitic impedances at the positive, negative, $y$, $x$ and $w$ terminals [40]. Considering
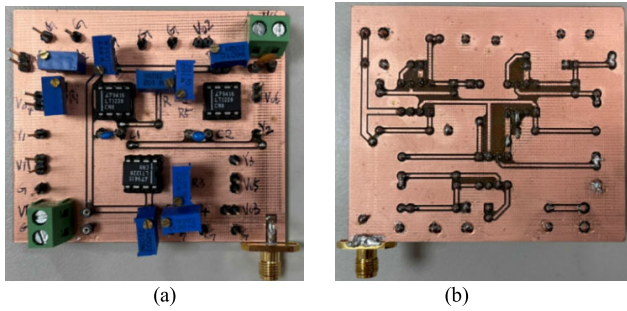
**FIGURE 6.** Second PCB prototype (a) top view and (b) bottom view of the measurement circuit in Fig. 3.
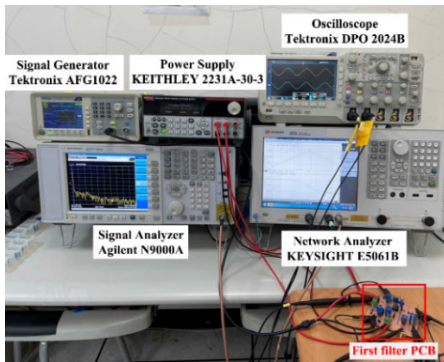


**FIGURE 7.** Experimental test bench for the first LT1228-based measurement circuit in Fig. 2.

the non-ideal LT1228 in Fig. 4, the finite input and output parasitic resistances and capacitances of the LT1228 will affect the two proposed LT1228-based circuits. The positive and negative terminals of the LT1228 exhibit the high value parasitic input resistances and low value capacitances of $R_{V+}$, $R_{V-}$, $C_{V+}$, and $C_{V-}$, respectively. The $y$ terminal of the LT1228 exhibits the high value parasitic output resistance and low value capacitance of $R_y$ and $C_y$, respectively. $R_T$ is a very high value parasitic input resistances, and $C_T$ is a low value parasitic capacitances of the LT1228. $R_x$ and $R_w$ are the low value parasitic output resistances at the low output impedance of the $x$ and $w$ terminals, respectively. Each proposed VM biquadratic filter uses two GCs in the circuit design to absorb the equivalent parallel parasitic capacitances of the LT1228s. To reduce the effect of the LT1228 parasitic elements on the performance of the two proposed LT1228-based filters, the external capacitors of $C_1$, $C_2$, $C_3$ and $C_4$ can be kept much larger than the $C_{V+}$, $C_{V-}$ and $C_y$ of the LT1228, the external resistors of $R$, $R_2$, $R_4$, $R_7$ and $R_9$ can be chosen much larger than $R_x$ of the LT1228, and the external resistors of $R_1$, $R_3$, $R_5$, $R_6$, $R_8$, and $R_{10}$ can be chosen much larger than $R_w$ of the LT1228.

## III. SIMULATION AND EXPERIMENTAL RESULTS OF THE TWO PROPOSED LT1228-BASED CIRCUITS
Based on the three off-the-shelf LT1228 ICs, the two proposed VM biquadratic filters of Figs. 2 and 3 were simulated
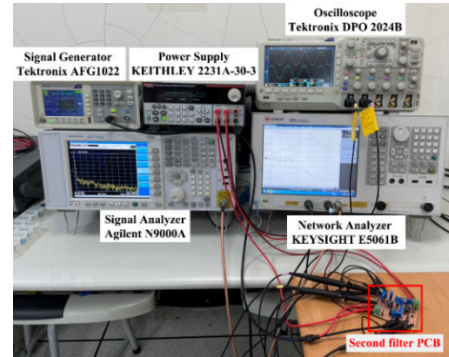


**FIGURE 8.** Experimental test bench for the second LT1228-based measurement circuit in Fig. 3.
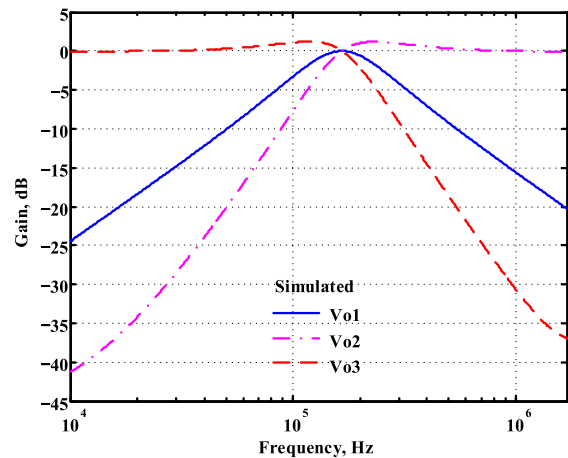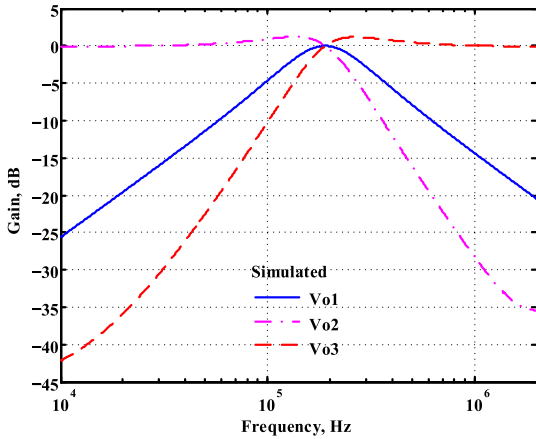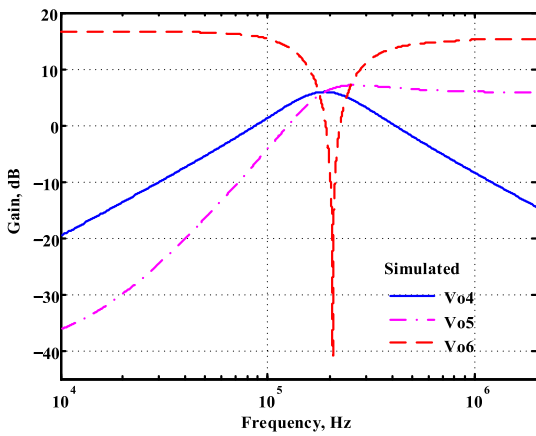


**FIGURE 9.** Simulated gain responses of $V_{o1}$, $V_{o2}$ and $V_{o3}$ for the first LT1228-based circuit in Fig. 2.
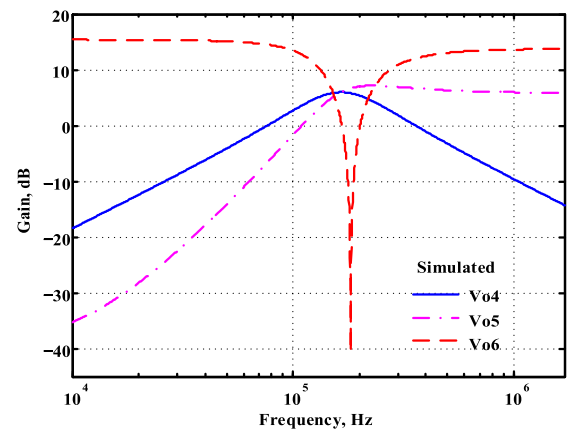


**FIGURE 10.** Simulated gain responses of $V_{o4}$, $V_{o5}$ and $V_{o6}$ for the first LT1228-based circuit in Fig. 2.

in the time and frequency domains using Cadence OrCAD Pspice, and their performances were experimentally verified using LT1228 ICs. Figures 5 and 6 show the experimental measurement photos of printed circuit boards (PCBs) of the two proposed LT1228-based filters in Figs. 2 and 3, respectively. Figures 7 and 8 show two experimental test benches,
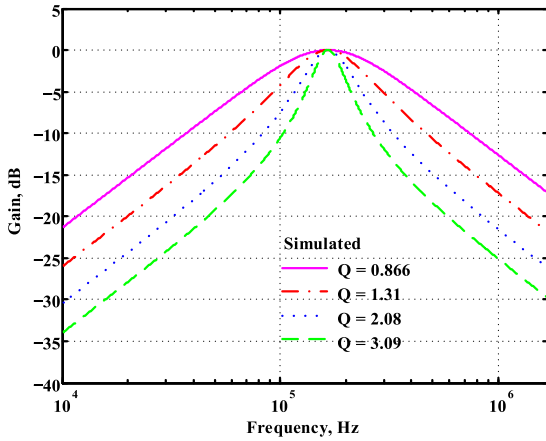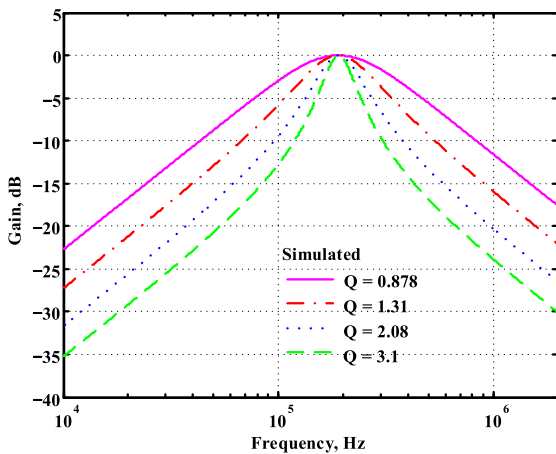
**FIGURE 11.** Simulated BP gain response results at $V_{o1}$ for the first LT1228-based circuit by using different DC bias currents for a fixed $f_o$ and only varying $Q$ value.
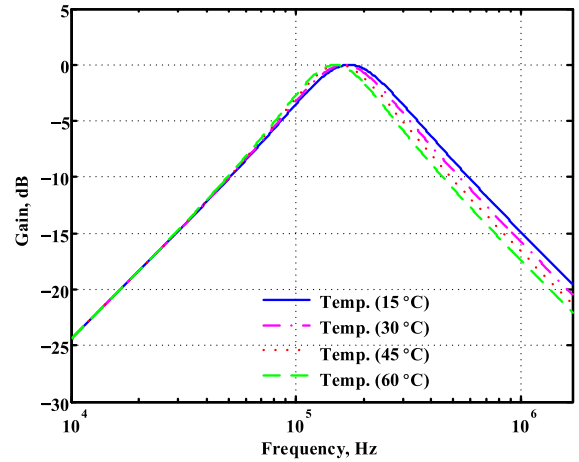


**FIGURE 13.** Simulated frequency domain at $V_{o1}$ for the first LT1228-based circuit with different temperature variations.
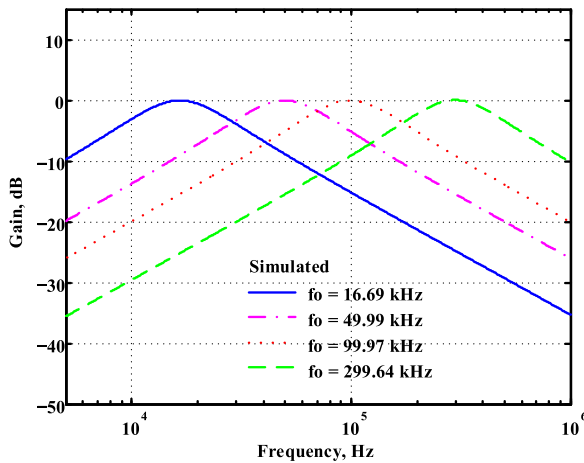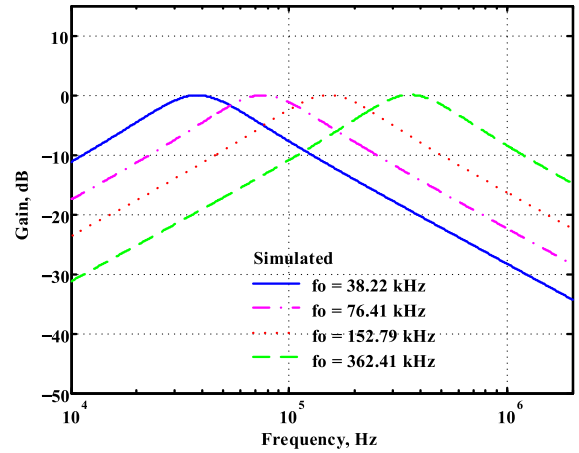


**FIGURE 12.** Simulated BP gain response results at $V_{o1}$ for the first LT1228-based circuit by using different DC bias currents for a fixed $Q$ and only varying $f_o$ value.
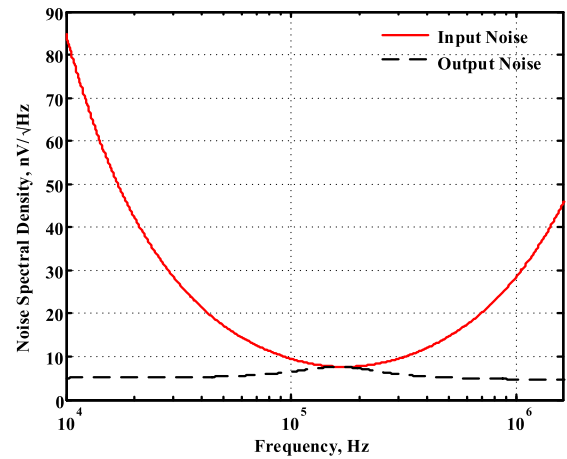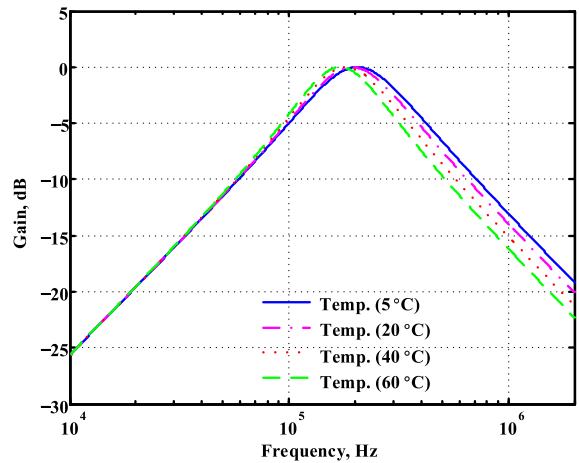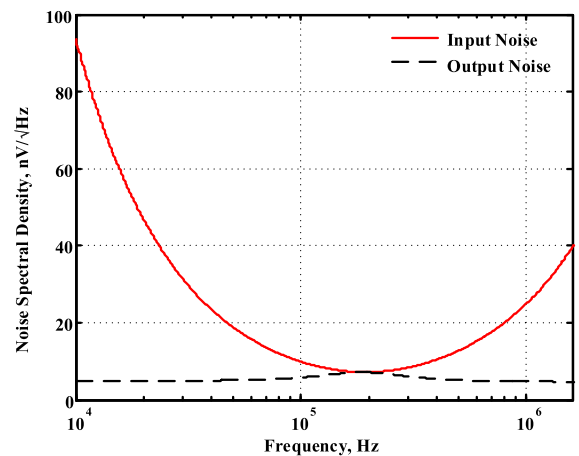


**FIGURE 14.** Simulated BP filter response at $V_{o1}$ for the first LT1228-based circuit Input and output noise variations.

**TABLE 5.** Summary of frequency analysis results for the first LT1228-based circuit simulated at ideal pole phase shift.

| First proposed filter responses | | Operating frequency at ideal pole phase shift | |
|---|---|---|---|
| Output terminal | Filter type | Simulated pole frequency value | Calculated frequency percentage error |
| $V_{o1}$ | BP response | 166.24 kHz | −1.81% |
| $V_{o2}$ | LP response | 166.02 kHz | −1.94% |
| $V_{o3}$ | HP response | 165.9 kHz | −2.01% |
| $V_{o4}$ | BP response | 166.06 kHz | −1.91% |
| $V_{o5}$ | HP response | 165.55 kHz | −2.22% |
| $V_{o6}$ | LPN response | 165.96 kHz | −1.97% |

**TABLE 6.** Summary of frequency analysis results for the second LT1228-based circuit simulated at ideal pole phase shift.

| Second proposed filter responses | | Operating frequency at ideal pole phase shift | |
|---|---|---|---|
| Output terminal | Filter type | Simulated pole frequency value | Calculated frequency percentage error |
| $V_{o1}$ | BP response | 190.33 kHz | −1.93% |
| $V_{o2}$ | LP response | 190.45 kHz | −1.87% |
| $V_{o3}$ | HP response | 190.1 kHz | −2.05% |
| $V_{o4}$ | BP response | 190.22 kHz | −1.99% |
| $V_{o5}$ | HP response | 189.81 kHz | −2.2% |
| $V_{o6}$ | LPN response | 190.22 kHz | −1.99% |

each including a power supply, signal generator, oscilloscope, signal analyzer, network analyzer, and the tested PCB circuit. According to [38] and the LT1228 datasheet [44], the LT1228 can be operated from any supply voltages from ±2 V to ±15 V. Low supply voltages can be used in biomedical sensor

systems and high supply voltages can be used in communication electronic systems. To obtain higher linearly, larger dynamic range (DR), and one-dB power gain compression point (P1dB), the symmetrical DC power supply voltages of the LT1228 were chosen to be ±15 V. Each power dissipation measured in Figs. 5 and 6 is 1.11 and 0.87 W, respectively.

**FIGURE 15.** Simulated gain responses of $V_{o1}$, $V_{o2}$ and $V_{o3}$ for the second LT1228-based circuit in Fig. 3.



**FIGURE 16.** Simulated gain responses of $V_{o4}$, $V_{o5}$ and $V_{o6}$ for the second LT1228-based circuit in Fig. 3.



**FIGURE 17.** Simulated BP gain response results at $V_{o1}$ for the second LT1228-based circuit by using different DC bias currents for a fixed $f_o$ and only varying $Q$ value.



**FIGURE 18.** Simulated BP gain response results at $V_{o1}$ for the second LT1228-based circuit by using different DC bias currents for a fixed $Q$ and only varying $f_o$ value.



**FIGURE 19.** Simulated frequency domain at $V_{o1}$ for the second LT1228-based circuit with different temperature variations.



**FIGURE 20.** Simulated BP filter response at $V_{o1}$ for the second LT1228-based circuit Input and output noise variations.

## A. PSPICE SIMULATION RESULTS OF THE FIRST LT1228-BASED CIRCUIT

The first proposed VM biquadratic filter was theoretically verified and functionally predicted using the Pspice macro-model of the LT1228. The components used in the first proposed VM biquadratic filter were chosen as $I_{B1} = I_{B2} = I_{B3} = 500\ \mu A$, $R = 0.2\ k\Omega$, $R_1 = R_2 = R_3 = R_4 = R_5 = 1\ k\Omega$, and $C_1 = C_2 = 4.7\ nF$ with an ideal pole frequency
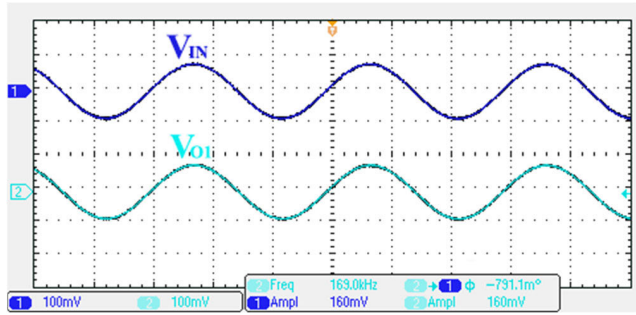
**FIGURE 21.** Measured transient response at $V_{o1}$ for the first LT1228-based circuit in Fig. 2.



**FIGURE 22.** Measured transient response at $V_{o2}$ for the first LT1228-based circuit in Fig. 2.



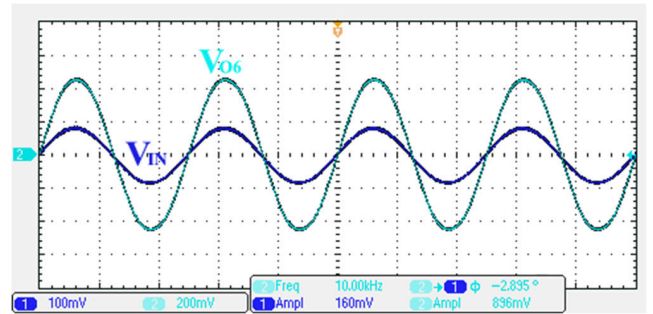**FIGURE 23.** Measured transient response at $V_{o3}$ for the first LT1228-based circuit in Fig. 2.



**FIGURE 24.** Measured transient response at $V_{o4}$ for the first LT1228-based circuit in Fig. 2.



**FIGURE 25.** Measured transient response at $V_{o5}$ for the first LT1228-based circuit in Fig. 2.



**FIGURE 26.** Measured transient response at $V_{o6}$ for the first LT1228-based circuit in Fig. 2.



**FIGURE 27.** Time domain LPN characteristics for the first circuit measured at a low-frequency of 10 kHz.
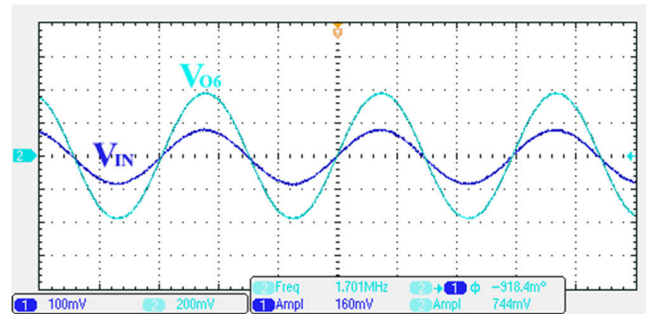


**FIGURE 28.** Time domain LPN characteristics for the first circuit measured at a high-frequency of 1.7 MHz.

of $f_o = 169.31$ kHz. Figures 9 and 10 represent the simulated gain responses of the six output voltages $V_{o1}$, $V_{o2}$, $V_{o3}$, $V_{o4}$, $V_{o5}$ and $V_{o6}$ in Fig. 2, respectively. Figures 11 and 12,

respectively, show the simulated electronic adjustment and independent control of the $f_o$ and $Q$ via their corresponding bias currents of the LT1228s, as described in (11). Table 5

**TABLE 7.** Summary of transient analysis results for the first LT1228-based circuit measured at the operating pole frequency.

| First proposed filter responses | | Operating pole frequency at $f_o$ = 169.31 kHz | | | |
|---|---|---|---|---|---|
| Output terminal | Filter type | Measured amplitude value | Calculated amplitude percentage error | Measured phase shift value | Calculated phase error |
| $V_{o1}$ | BP response | 160m $V_{PP}$ | 0% | −0.791° | −0.791° |
| $V_{o2}$ | LP response | 152m $V_{PP}$ | −0.05% | −90.61° | −0.61° |
| $V_{o3}$ | HP response | 160m $V_{PP}$ | 0% | −90.76° | −0.76° |
| $V_{o4}$ | BP response | 320m $V_{PP}$ | 0% | −0.243° | −0.243° |
| $V_{o5}$ | HP response | 328m $V_{PP}$ | 0.025% | −90.88° | −0.88° |

**TABLE 8.** Summary of LPN transient analysis results for the first LT1228-based circuit measured at low and high frequencies.

| LPN transient analysis of the $V_{o6}$ output voltage | | | |
|---|---|---|---|
| Operating at a low-frequency of 10 kHz | | | |
| Measured amplitude value | Percentage error of amplitude | Measured phase shift value | Calculated phase error |
| 896m $V_{pp}$ | −6.66% | −2.89° | −0.5° |
| Operating at a high-frequency of 1.7 MHz | | | |
| Measured amplitude value | Calculated amplitude percentage error | Measured phase shift value | Calculated phase error |
| 744m $V_{pp}$ | −7% | −0.918° | 6.68° |



**FIGURE 29.** Measured frequency domain at $V_{o1}$ for the first LT1228-based circuit in Fig. **2**.
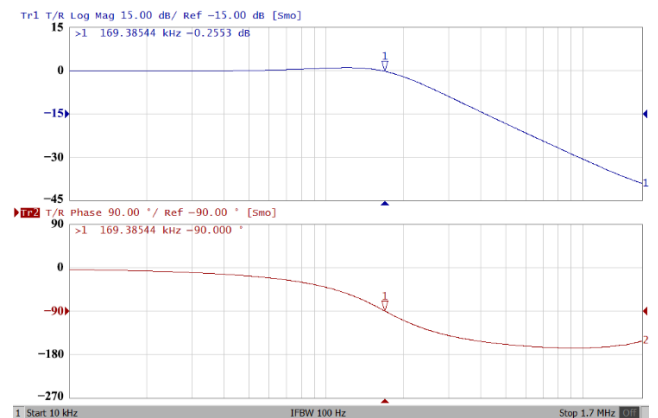


**FIGURE 30.** Measured frequency domain at $V_{o2}$ for the first LT1228-based circuit in Fig. **2**.
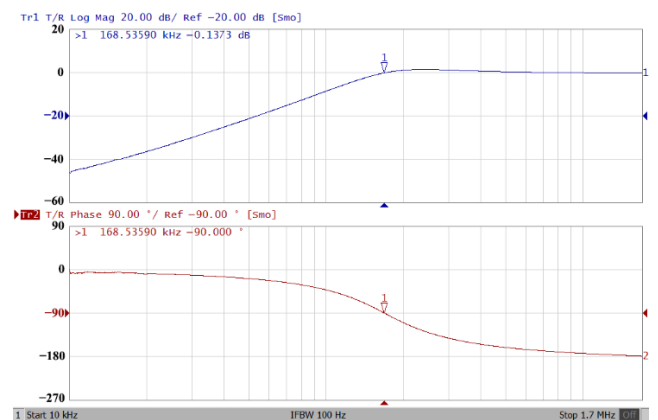


**FIGURE 31.** Measured frequency domain at $V_{o3}$ for the first LT1228-based circuit in Fig. **2**.

summarizes the simulation results of the first LT1228-based circuit, compared with the deviation from the ideal pole frequency $f_o$ = 169.31 kHz. These simulation results confirm the functional predictions of the first LT1228-based circuit. To evaluate the effect of temperature changes, the first proposed circuit was simulated for different temperature variations. In this analysis, the simulated temperature changes were set to 15°C, 30°C, 45°C, and 60°C, respectively. Figure 13 demonstrates the simulated frequency domain for different temperature variations. In Fig. 13, this change does not have much effect on the frequency domain of the filter. However, at an operating frequency of $f_o$ = 169.31 kHz, the $f_o$ values deviate by 172.76 kHz, 164.76 kHz, 156.91 kHz, and 149.85 kHz at 15°C, 30°C, 45°C, and 60°C, respectively. Figure 14 demonstrates the simulated input and output noises of the first proposed LT1228-based filter at $V_{o1}$. As shown in Fig. 14, the input and output noises of the first proposed LT1228-based filter at $V_{o1}$ are low values.

## B. PSPICE SIMULATION RESULTS OF THE SECOND LT1228-BASED CIRCUIT

The components used in the second proposed VM biquadratic filter were chosen as $I_{B4} = I_{B5} = I_{B6} = 1000\ \mu A$, $R = 0.1$ kΩ, $R_6 = R_7 = R_8 = R_9 = 1$ kΩ, $R_{10} = 0.6$ kΩ, and $C_3 = C_4 = 8.2$ nF with an ideal pole frequency of $f_o$ = 194.09 kHz. Figures 15 and 16 represent the simulated gain

responses of the six output voltages $V_{o1}$, $V_{o2}$, $V_{o3}$, $V_{o4}$, $V_{o5}$ and $V_{o6}$ in Fig. 3, respectively. Figures 17 and 18, respectively, show the simulated electronic adjustment and independent control of the $f_o$ and $Q$ via their corresponding bias currents of the LT1228s, as described in (24). Table 6 summarizes the simulation results of the second LT1228-based
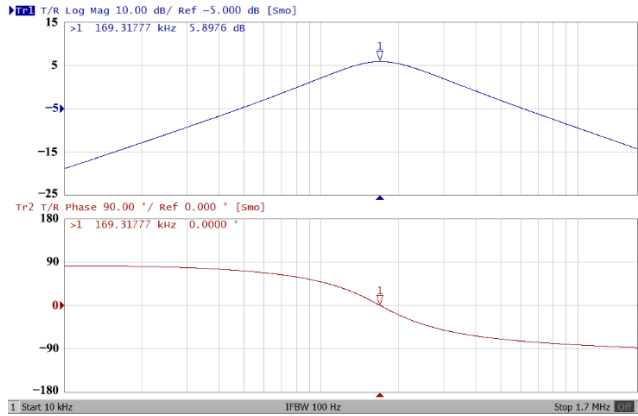
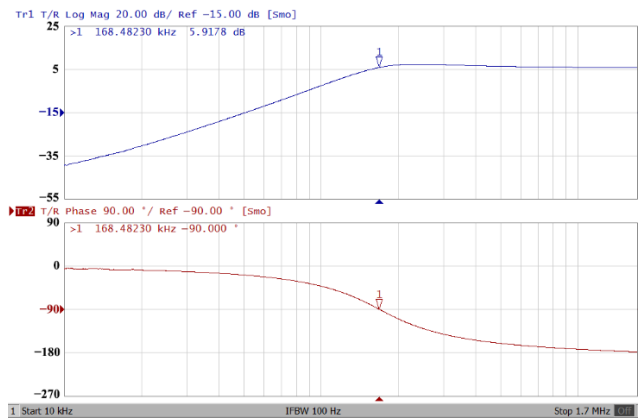**FIGURE 32.** Measured frequency domain at $V_{o4}$ for the first LT1228-based circuit in Fig. 2.



**FIGURE 33.** Measured frequency domain at $V_{o5}$ for the first LT1228-based circuit in Fig. 2.
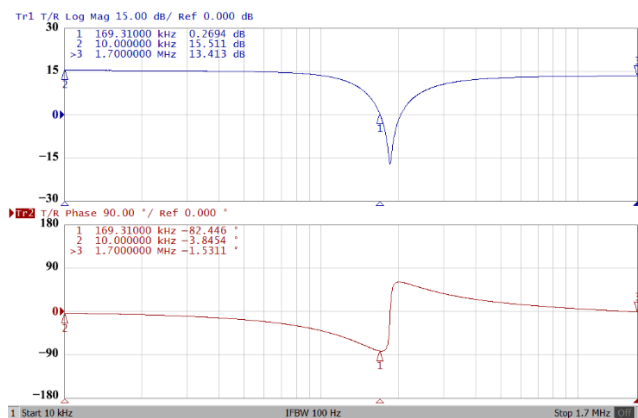


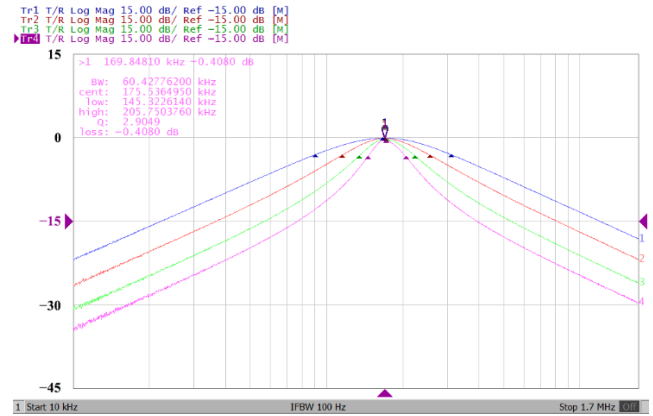**FIGURE 34.** Measured frequency domain at $V_{o6}$ for the first LT1228-based circuit in Fig. 2.



**FIGURE 35.** Measured BP gain response results at $V_{o1}$ for the first LT1228-based circuit by using different DC bias currents for a fixed $f_o$ and only varying Q value.
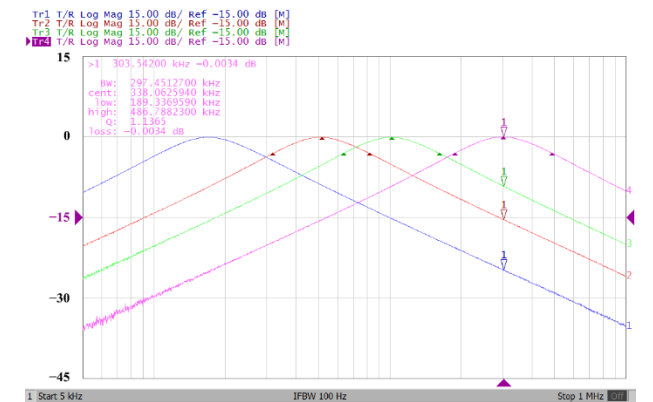


**FIGURE 36.** Measured BP gain response results at $V_{o1}$ for the first LT1228-based circuit by using different DC bias currents for a fixed Q value and only varying $f_o$.

**TABLE 9.** Summary of frequency analysis results for the first LT1228-based circuit measured at ideal pole phase shift.

| First proposed filter responses | | Operating frequency at the ideal pole phase shift | |
|---|---|---|---|
| Output terminal | Filter type | Measured pole frequency value | Calculated frequency percentage error |
| $V_{o1}$ | BP response | 168.3 kHz | −0.59% |
| $V_{o2}$ | LP response | 169.38 kHz | 0.04% |
| $V_{o3}$ | HP response | 168.53 kHz | −0.46% |
| $V_{o4}$ | BP response | 169.31 kHz | 0% |
| $V_{o5}$ | HP response | 168.48 kHz | 0.49% |

circuit, compared with the deviation from the ideal pole frequency $f_o = 194.09$ kHz. These simulation results confirm the functional predictions of the second LT1228-based circuit. To evaluate the effect of temperature changes, the second proposed circuit was simulated for different temperature variations. Figure 19 demonstrates the simulated frequency domain for different temperature variations. In Fig. 19, this change does not have much effect on the frequency domain of the filter. However, at an operating frequency of $f_o = 194.09$ kHz, the $f_o$ values deviate by 205.45 kHz, 195.42 kHz, 182.46 kHz, and 171.55 kHz at 5°C, 20°C, 40°C, and 60°C, respectively. Figure 20 demonstrates the simulated input and output noises of the second proposed LT1228-based filter at $V_{o1}$. As shown in Fig. 20, the input and output noises of the second proposed LT1228-based filter at $V_{o1}$ are low values.
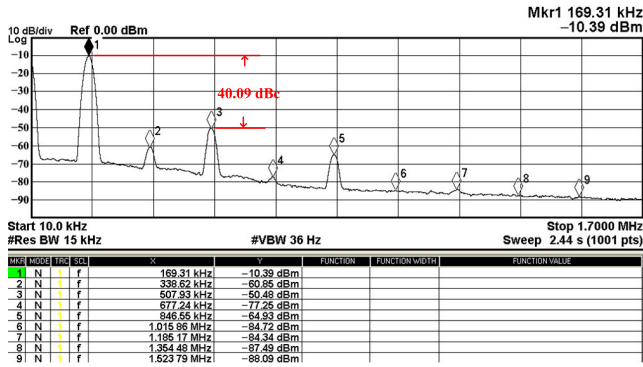
**FIGURE 37.** Measured spectrum analysis results at $V_{o1}$ for the first LT1228-based circuit in Fig. 2.
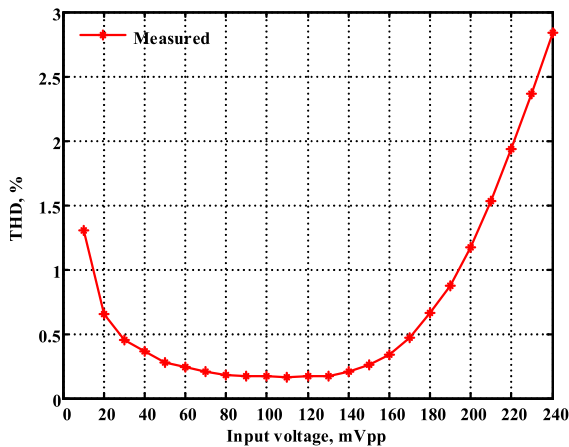


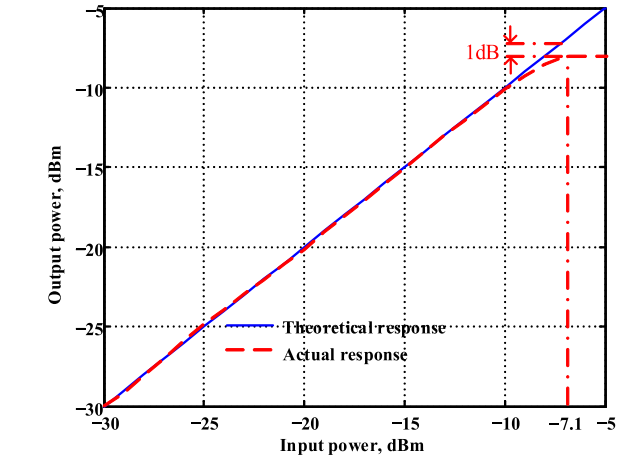**FIGURE 38.** Measured THD analysis results at $V_{o1}$ for the first LT1228-based circuit in Fig. 2.



**FIGURE 39.** Measured noise analysis results at $V_{o1}$ for the first LT1228-based circuit in Fig. 2.



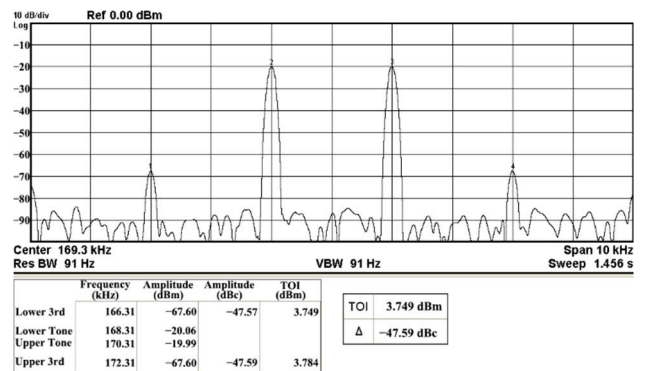**FIGURE 40.** Measured P1dB results at $V_{o1}$ for the first circuit in Fig. 2.



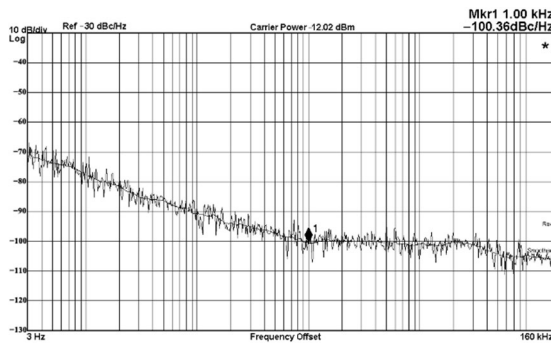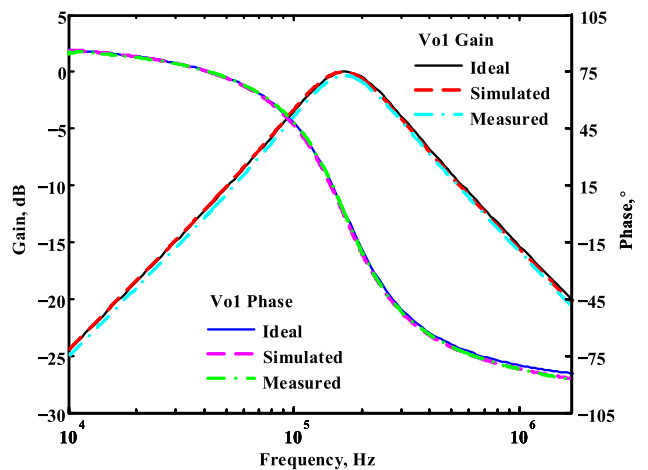**FIGURE 41.** Measured IMD results at $V_{o1}$ for the first circuit in Fig. 2.



**FIGURE 42.** Frequency domain simulation and measurement results at $V_{o1}$ for the first LT1228-based circuit compared with theoretical analysis using Matlab software.

## C. EXPERIMENTAL RESULTS OF THE FIRST LT1228-BASED CIRCUIT

Based on three off-the-shelf LT1228 ICs, the first proposed VM biquadratic filter is implemented to experimentally demonstrate the feasibility and practicality of the circuit. The circuit was measured in both time and frequency domains, using the same values for transconductance, resistance, and capacitance elements as in Section III-A. Figures 21 to 26,

respectively, show the measured transient responses of $V_{o1}$, $V_{o2}$, $V_{o3}$, $V_{o4}$, $V_{o5}$ and $V_{o6}$ in Fig. 2 at $f_o$ = 169.31 kHz operating frequency. Figures 27 and 28 show the time-domain characteristics of the LPN filter operating at
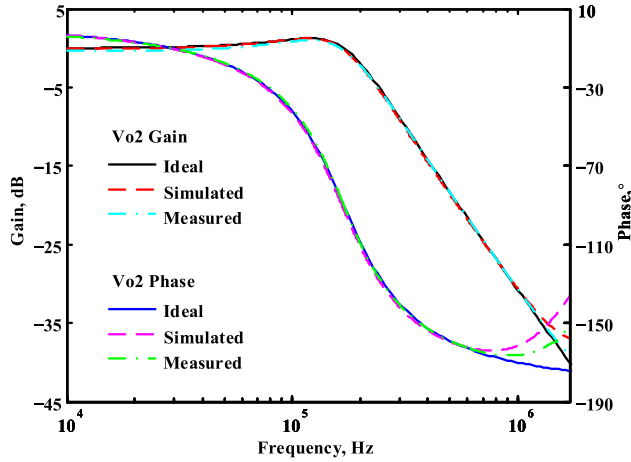
**FIGURE 43.** Frequency domain simulation and measurement results at $V_{O2}$ for the first LT1228-based circuit compared with theoretical analysis using Matlab software.



**FIGURE 44.** Frequency domain simulation and measurement results at $V_{O3}$ for the first LT1228-based circuit compared with theoretical analysis using Matlab software.



**FIGURE 45.** Frequency domain simulation and measurement results at $V_{O4}$ for the first LT1228-based circuit compared with theoretical analysis using Matlab software.
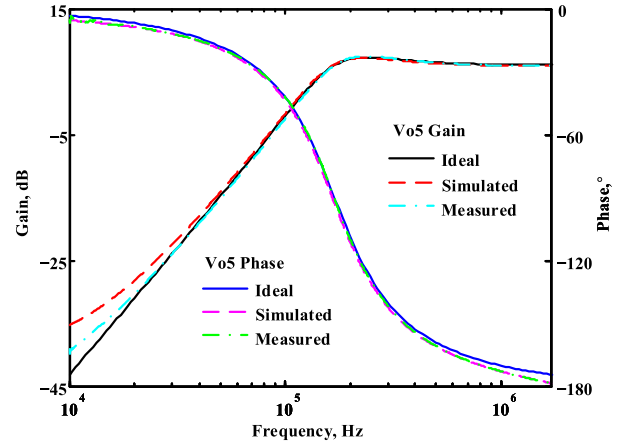


**FIGURE 46.** Frequency domain simulation and measurement results at $V_{O5}$ for the first LT1228-based circuit compared with theoretical analysis using Matlab software.
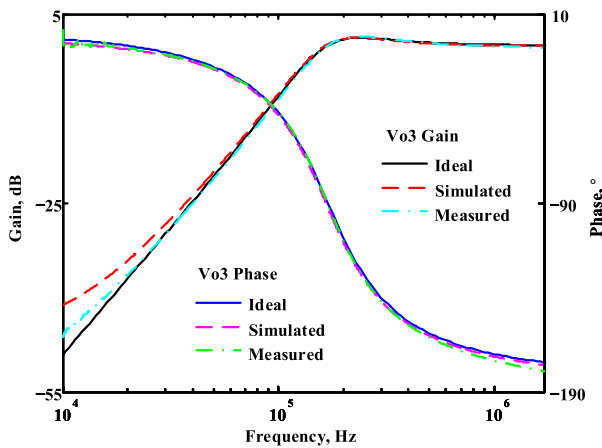


**FIGURE 47.** Frequency domain simulation and measurement results at $V_{O6}$ for the first LT1228-based circuit compared with theoretical analysis using Matlab software.
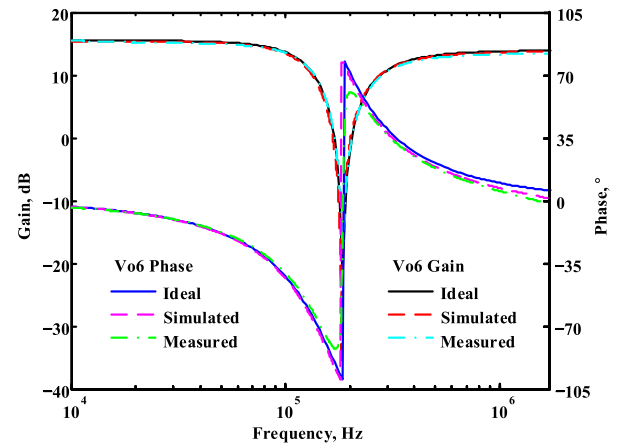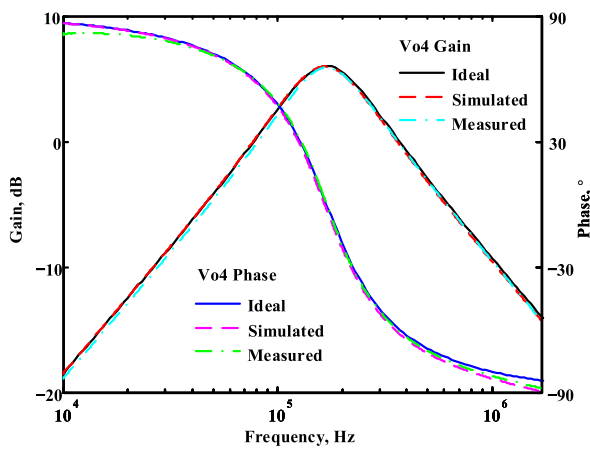


**FIGURE 48.** Simulated, measured and theoretical BP gain response results at $V_{O1}$ for the first LT1228-based circuit by using different DC bias currents for a fixed $f_o$ and only varying $Q$ value.

a low-frequency of 10 kHz and a high-frequency of 1.7 MHz, respectively. Table 7 summarizes the measured transient response results of the first LT1228-based circuit at the ideal operating pole frequency $f_o$ = 169.31 kHz. Table 8 summarizes the measured transient response results of the LPN operating at a low-frequency of 10 kHz and a high-frequency
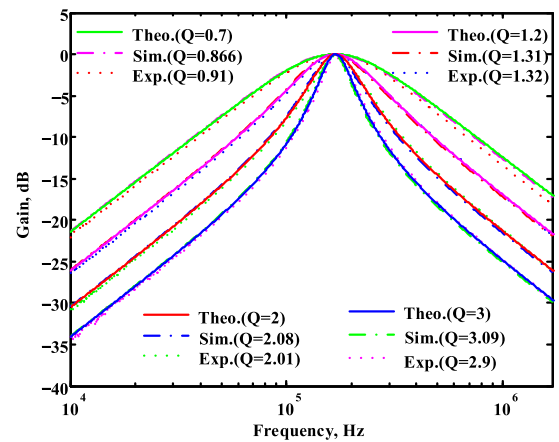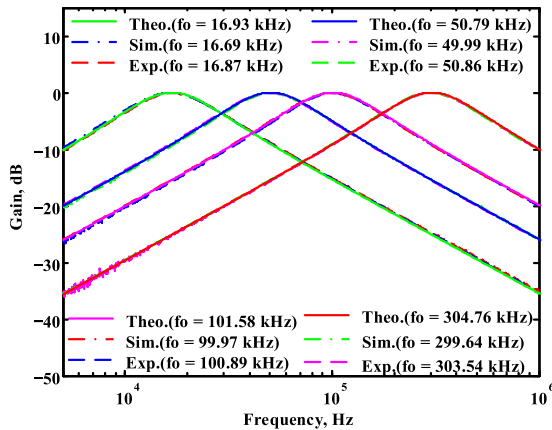
**FIGURE 49.** Simulated, measured and theoretical BP gain response results at $V_{o1}$ for the first LT1228-based circuit by using different DC bias currents for a fixed $Q$ and only varying $f_o$ value.



**FIGURE 50.** Frequency domain simulation and measurement results at $V_{o1}$ for the second LT1228-based circuit compared with theoretical analysis using Matlab software.



**FIGURE 51.** Frequency domain simulation and measurement results at $V_{o2}$ for the second LT1228-based circuit compared with theoretical analysis using Matlab software.



**FIGURE 52.** Frequency domain simulation and measurement results at $V_{o3}$ for the second LT1228-based circuit compared with theoretical analysis using Matlab software.

of 1.7 MHz, respectively. The measured transient responses in Figs. 21 to 28, Tables 7 and 8 demonstrate the validity and practicality of the theoretical structural analysis of the first LT1228-based circuit. To show the frequency-domain of the first LT1228-based circuit, the gain and phase frequency responses were performed. Figures 29 to 34 represent the measured gain and phase responses of the six output voltages $V_{o1}$, $V_{o2}$, $V_{o3}$, $V_{o4}$, $V_{o5}$ and $V_{o6}$ in Fig. 2, respectively. Table 9 summarizes the measured frequency analysis results of the first LT1228-based circuit, compared with the deviation from the ideal pole frequency $f_o = 169.31$ kHz. Figure 35 shows the $Q$ values measured without disturbing $f_o$. The $f_o$ measured without disturbing $Q$ values was shown in Fig. 36. The measured frequency responses in Figs. 29 to 36, and Table 9 demonstrate the validity and practicality of the theoretical structural analysis of the first LT1228-based circuit. These measurements verify the real performance of the first LT1228-based circuit.

To determine the total harmonic distortion (THD) of the first LT1228-based circuit, the output signal spectrum was analyzed. Figure 37 shows the output spectrum analysis at $V_{o1}$ for the first LT1228-based circuit with an input voltage amplitude of 192m $V_{pp}$. In Fig. 37, the first LT1228-based circuit has a measured spurious-free dynamic range (SFDR) of approximately 40.09 dBc at 1% THD. Figure 38 shows the THD analysis at $V_{o1}$ for different input voltage amplitudes, and the THD results remain below 2% when the input voltage is increased by 220m $V_{pp}$. Figure 39 shows the noise analysis results at $V_{o1}$ for the first LT1228-based circuit. The phase noise measured at $V_{o1}$ for the first LT1228-based circuit is lower than $-100.36$ dBc/Hz (at 1 kHz offset).
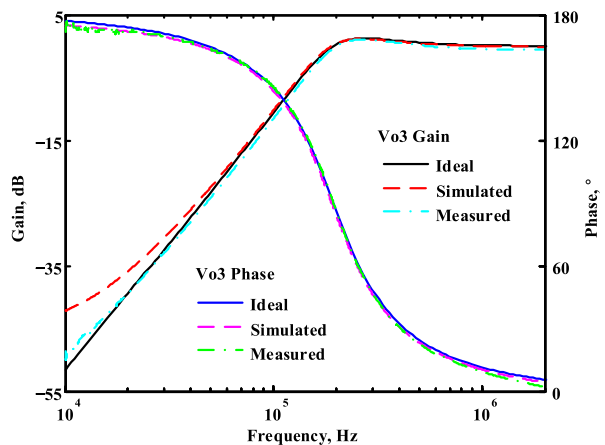
To evaluate the linearity and nonlinearity performance at $V_{o1}$ for the first LT1228-based circuit, two-tone testing of intermodulation distortion (IMD) and P1dB were performed. Figures 40 and 41 show the measured results of the P1dB and IMD tests at $V_{o1}$ for the first LT1228-based circuit, respectively. In Fig. 40, the input P1dB point measured at $V_{o1}$ for the first LT1228-based circuit is approximately
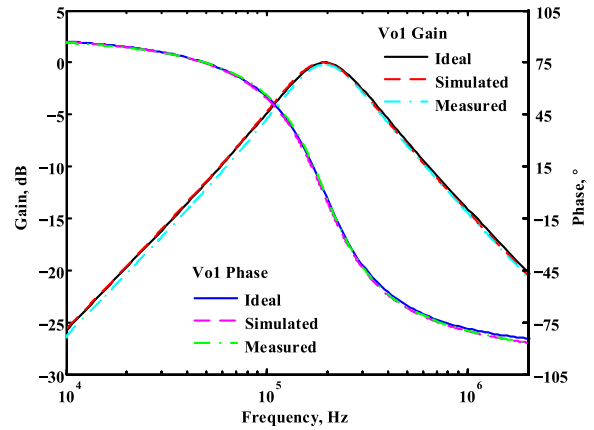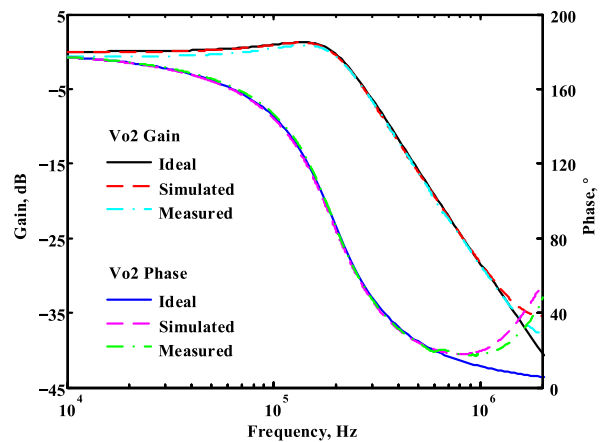
$-7.1$ dBm. In Fig. 41, the third-order IMD (IMD3) and third-order intercept (TOI) point measured at $V_{o1}$ for the first LT1228-based circuit are $-47.59$ dBc and 3.749 dBm, respectively.
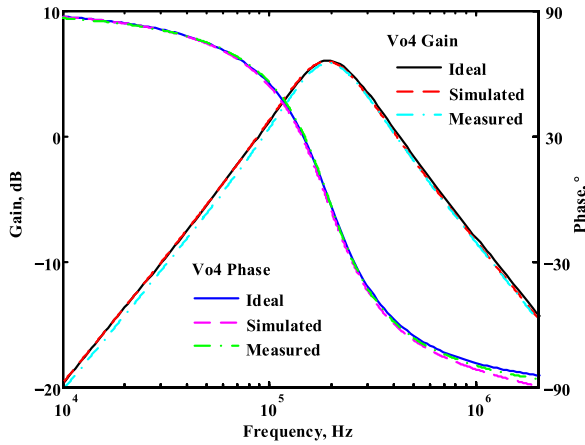
**FIGURE 53.** Frequency domain simulation and measurement results at $V_{o4}$ for the second LT1228-based circuit compared with theoretical analysis using Matlab software.



**FIGURE 54.** Frequency domain simulation and measurement results at $V_{o5}$ for the second LT1228-based circuit compared with theoretical analysis using Matlab software.



**FIGURE 55.** Frequency domain simulation and measurement results at $V_{o6}$ for the second LT1228-based circuit compared with theoretical analysis using Matlab software.
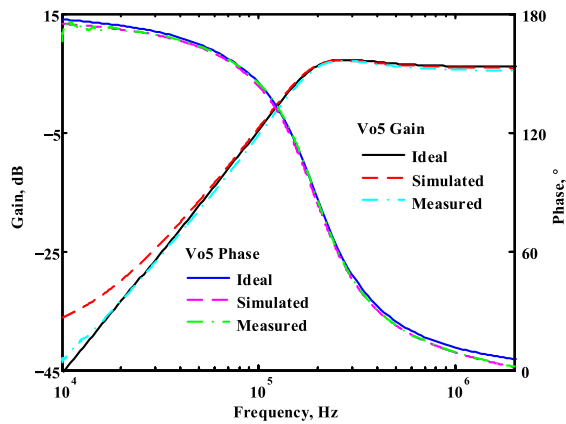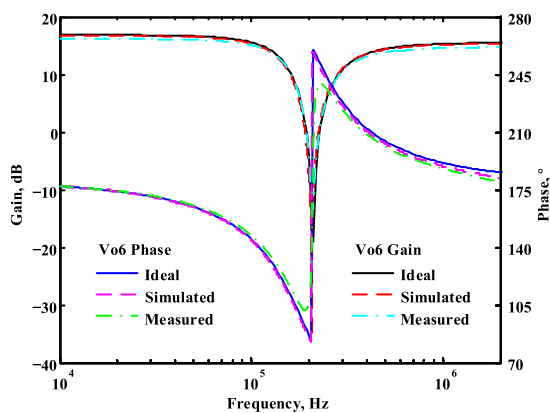
## D. THEORETICAL COMPARISON OF THE FIRST LT1228-BASED CIRCUIT WITH SIMULATION AND EXPERIMENTAL RESULTS

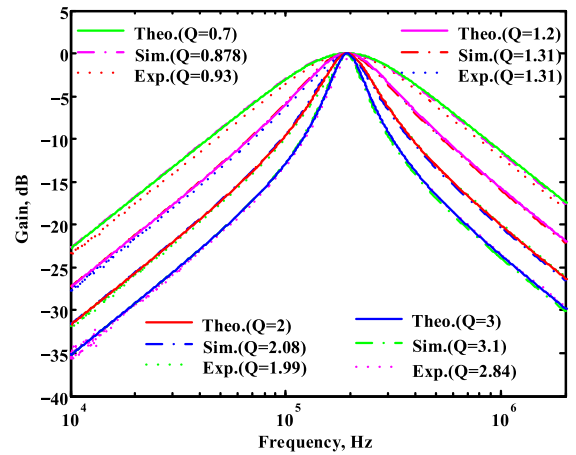To verify the performance of the first LT1228-based circuit, simulation and experimental data results were analyzed



**FIGURE 56.** Simulated, measured and theoretical BP gain response results at $V_{o1}$ for the second LT1228-based circuit by using different DC bias currents for a fixed $f_o$ and only varying $Q$ value.
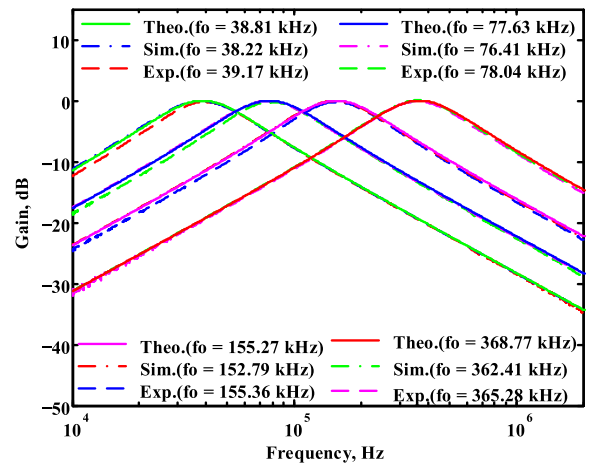


**FIGURE 57.** Simulated, measured and theoretical BP gain response results at $V_{o1}$ for the first LT1228-based circuit by using different DC bias currents for a fixed $Q$ and only varying $f_o$ value.

**TABLE 10.** Summary of the frequency analysis results for the second LT1228-based circuit measured at ideal pole phase shift.

| Second proposed filter responses | | Operating frequency at the ideal pole phase shift | |
|---|---|---|---|
| Output terminal | Filter type | Measured pole frequency value | Calculated frequency percentage error |
| $V_{o1}$ | BP response | 193.99 kHz | 0.05% |
| $V_{o2}$ | LP response | 193.73 kHz | 0.18% |
| $V_{o3}$ | HP response | 194.09 kHz | 0% |
| $V_{o4}$ | BP response | 194.05 kHz | 0.02% |
| $V_{o5}$ | HP response | 193.23 kHz | 0.44% |

using Matlab version R2014a software and compared with circuit theory. Figures 42 to 47 represent the gain and phase responses of the six output voltages $V_{o1}$, $V_{o2}$, $V_{o3}$, $V_{o4}$, $V_{o5}$ and $V_{o6}$ in Fig. 2, respectively, and compare them with theoretical, simulated and measured values. Figures 48 and 49 illustrate the ability to control $f_o$ and $Q$ electronically and independently by the bias currents of their corresponding LT1228s, as described in (11). As shown in Figs. 42 to 49,

**FIGURE 58.** Measured spectrum analysis results at $V_{o1}$ for the second LT1228-based circuit in Fig. 3.



**FIGURE 59.** Measured THD analysis results at $V_{o1}$ for the second LT1228-based circuit in Fig. 3.
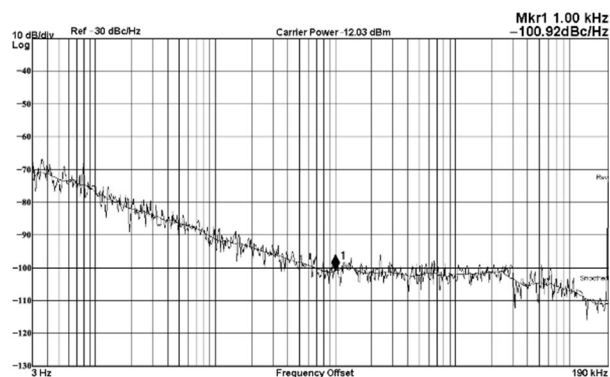


**FIGURE 60.** Measured noise analysis results at $V_{o1}$ for the second LT1228-based circuit in Fig. 3.
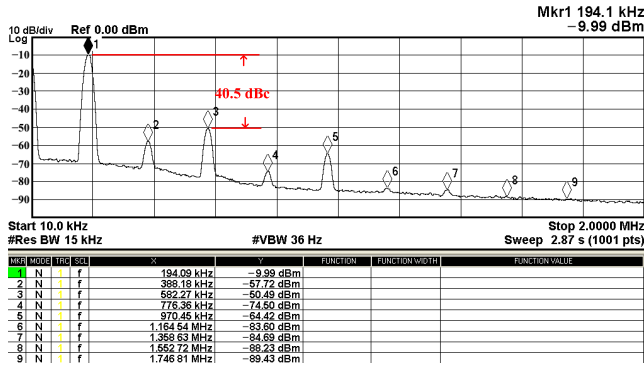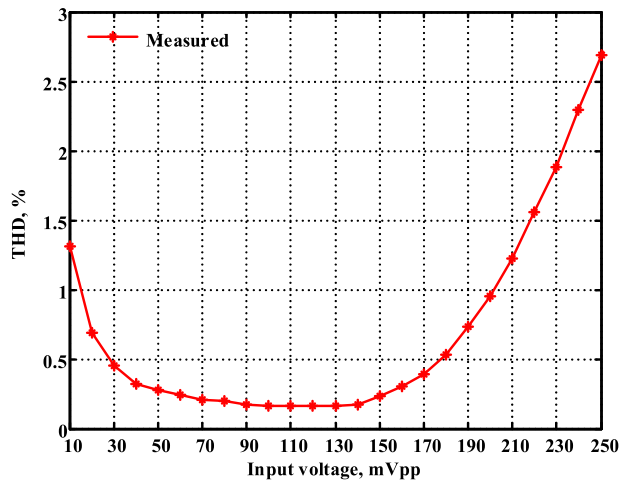
these results for the first LT1228-based circuit are in good agreement with theoretical predictions. However, the differences between the theoretical, simulated and measured responses are mainly due to non-ideal characteristics of the circuit, tolerances in capacitance and resistance, and PCB layout performance.
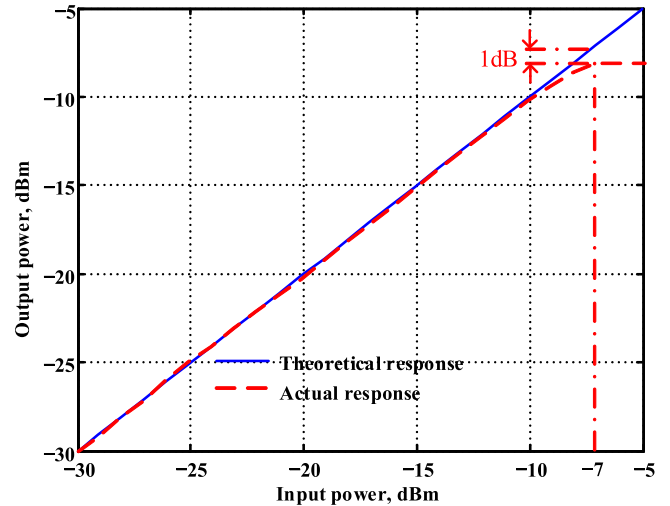
**FIGURE 61.** Measured P1dB results at $V_{o1}$ for the second LT1228-based circuit in Fig. 3.
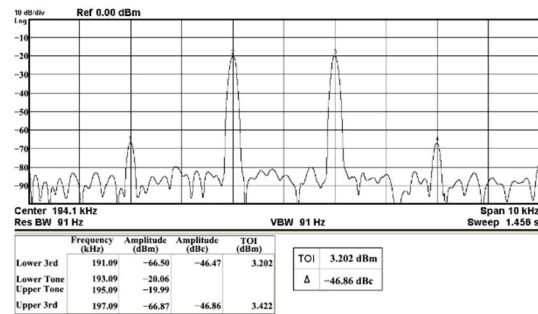


**FIGURE 62.** Measured IMD results at $V_{o1}$ for the second LT1228-based circuit in Fig. 3.

### E. THEORETICAL COMPARISON OF THE SECOND LT1228-BASED CIRCUIT WITH SIMULATION AND EXPERIMENTAL RESULTS

Similarly, the second proposed LT1228-based circuit is also measured in frequency-domain using the same values for transconductance, resistance, and capacitance elements as in Section III-B. Figures 50 to 55 represent the gain and phase responses of the six output voltages $V_{o1}$, $V_{o2}$, $V_{o3}$, $V_{o4}$, $V_{o5}$ and $V_{o6}$ in Fig. 3 compared to ideal, simulated, and measured values using Matlab version R2014a software, respectively. In Figs. 50 to 55, the second LT1228-based circuit also operated well as expected. Figures 56 and 57 illustrate the ability to control $f_o$ and $Q$ electronically and independently by the bias currents of their corresponding LT1228s, as described in (24). Table 10 summarizes the measured frequency analysis results of the second LT1228-based circuit, compared with the deviation from the ideal pole frequency $f_o = 194.09$ kHz. The measured frequency responses in Figs. 50 to 57, and Table 10 demonstrate the validity and practicality of the theoretical structure analysis of the second LT1228-based circuit.

To determine the THD of the second LT1228-based circuit, the output signal spectrum was analyzed. Figure 58 shows the output spectrum analysis at $V_{o1}$ for the second LT1228-based circuit with an input voltage amplitude of 205m $V_{pp}$. In Fig. 58, the second LT1228-based circuit has a measured SFDR of approximately 40.5 dBc at 1% THD. Figure 59 shows the THD analysis at $V_{o1}$ for different input voltage amplitudes, and the THD results remain below 2% when the input voltage is increased by 230m $V_{pp}$. Figure 60 shows the noise analysis results at $V_{o1}$ for the second LT1228-based circuit. The phase noise measured at $V_{o1}$ for the second LT1228-based circuit is lower than $-100.92$ dBc/Hz (at 1 kHz offset). Figures 61 and 62 show the measured results of the P1dB and IMD tests at $V_{o1}$ for the second LT1228-based circuit, respectively. In Fig. 61, the input P1dB point measured at $V_{o1}$ for the second LT1228-based circuit is approximately $-7$ dBm. In Fig. 62, the IMD3 and TOI point measured at $V_{o1}$ for the second LT1228-based circuit are $-46.86$ dBc and 3.202 dBm, respectively.

## IV. CONCLUSION

To achieve independent gain control of BP, HP, and LPN/RN filters, this paper presents two new and improved VM biquadratic filters using three commercial LT1228 ICs, two GCs, and six resistors. Each electronically adjustable VM biquadratic filter has a single input and six output voltages, designed to implement one LP, two BP, two HP and one LPN/RN filters simultaneously. Each VM biquadratic filter has one high input impedance and three low output impedances with independent gain controllability for the BP, HP, and LPN/RN transfer functions. Due to its high input impedance and low output impedance, each proposed filter is suitable for cascaded VM circuits without the use of any voltage buffers. The $\omega_o$ and $Q$ of each filter parameter can be electronically controlled and orthogonally tuned by the corresponding LT1228 bias current $I_B$. In special cases, $\omega_o$ and $Q$ of each filter parameter can be made electronically controlled and independently adjustable. In electronic applications, each filter simultaneously generates one LP, two BP and two HP filters for use in two/three-way crossover networks. The LPN filter is also suitable for EEG applications to eliminate unwanted narrow frequency intervals in the signal. Simulation and experimental results in both time and frequency domains are included to validate the theoretical analysis of the two proposed VM biquadratic filters. Based on a $\pm 15$ V voltage supply, the measured power dissipation, P1dB, TOI, IMD3, SFDR, and phase noise of the first proposed VM biquadratic filter are 1.11 W, $-7.1$ dBm, 3.749 dBm, $-47.59$ dBc, 40.09 dBc, $-100.36$ dBc/Hz, respectively. The measured power dissipation, P1dB, TOI, IMD3, SFDR, and phase noise of the second proposed VM biquadratic filter are 0.87 W, $-7$ dBm, 3.202 dBm, $-46.86$ dBc, 40.5 dBc, and $-100.92$ dBc/Hz, respectively. The results show that the two proposed VM biquadratic filters achieve good performance.

## REFERENCES

[1] D. Biolek, R. Senani, V. Biolkova, and Z. Kolka, "Active elements for analog signal processing: Classification, review, and new proposals," *Radioengineering*, vol. 17, no. 4, pp. 15–32, Dec. 2008.

[2] T. S. Arora and A. K. Singh, "A new voltage mode sinusoidal quadrature oscillator employing second generation voltage conveyor," *AEU Int. J. Electron. Commun.*, vol. 154, Sep. 2022, Art. no. 154304.

[3] M. Kumngern, F. Khateb, P. Phatsornsiri, W. Jongchanachavawat, T. Kulej, U. Torteanchai, and M. Rattanasuttikan, "1.2 V differential difference current conveyor using MIGD MOST technique and its applications," *AEU Int. J. Electron. Commun.*, vol. 158, Jan. 2023, Art. no. 154445.

[4] P. Moonmuang, M. Faseehuddin, T. Pukkalanun, N. Herencsar, and W. Tangsrirat, "VDTA-based floating/grounded series/parallel R-L and R-C immittance simulators with a single grounded capacitor," *AEU Int. J. Electron. Commun.*, vol. 160, Feb. 2023, Art. no. 154502.

[5] R. Sotner, J. Jerabek, L. Polak, R. Theumer, and L. Langhammer, "Electronic tunability and cancellation of serial losses in wire coils," *Sensors*, vol. 22, no. 19, p. 7373, Sep. 2022.

[6] A. Abaci, H. Alpaslan, and E. Yuce, "First-order all-pass filters comprising one modified DDCC," *J. Circuits, Syst. Comput.*, vol. 31, no. 10, Jul. 2022, Art. no. 2250184.

[7] T. Yucehan and E. Yuce, "CCII-based voltage-mode and current-mode high-order filters with gains and grounded passive elements only," *AEU Int. J. Electron. Commun.*, vol. 155, Oct. 2022, Art. no. 154346.

[8] A. Raj, D. R. Bhaskar, R. Senani, and P. Kumar, "Extension of recently proposed two-CFOA-GC all pass filters to the realisation of first order universal active filters," *AEU Int. J. Electron. Commun.*, vol. 146, Mar. 2022, Art. no. 154119.

[9] H.-P. Chen, S.-F. Wang, Y. Ku, Y.-C. Yi, Y.-F. Li, and Y.-H. Chen, "Four unity/variable gain first-order cascaded voltage-mode all-pass filters and their fully uncoupled quadrature sinusoidal oscillator applications," *Sensors*, vol. 22, no. 16, p. 6250, Aug. 2022.

[10] P. Prommee, K. Karawanich, F. Khateb, and T. Kulej, "Voltage-mode elliptic band-pass filter based on multiple-input transconductor," *IEEE Access*, vol. 9, pp. 32582–32590, 2021.

[11] M. Kumngern, N. Aupithak, F. Khateb, and T. Kulej, "0.5 V fifth-order Butterworth low-pass filter using multiple-input OTA for ECG applications," *Sensors*, vol. 20, no. 24, p. 7343, Dec. 2020.

[12] E. Yuce, R. Verma, N. Pandey, and S. Minaei, "New CFOA-based first-order all-pass filters and their applications," *AEU Int. J. Electron. Commun.*, vol. 103, pp. 57–63, May 2019.

[13] P. K. Sharma, R. K. Ranjan, F. Khateb, and M. Kumngern, "Charged controlled mem-element emulator and its application in a chaotic system," *IEEE Access*, vol. 8, pp. 171397–171407, 2020.

[14] M. Kumngern, F. Khateb, and T. Kulej, "0.5 V current-mode low-pass filter based on voltage second generation current conveyor for bio-sensor applications," *IEEE Access*, vol. 10, pp. 12201–12207, 2022.

[15] F. Khateb, T. Kulej, M. Akbari, and M. Kumngern, "0.5-V high linear and wide tunable OTA for biomedical applications," *IEEE Access*, vol. 9, pp. 103784–103794, 2021.

[16] M. Kumngern, F. Khateb, and C. Psychalinos, "Multiple-input universal filter and quadrature oscillator using multiple-input operational transconductance amplifiers," *IEEE Access*, vol. 9, pp. 56253–56263, 2021.

[17] F. Khateb, M. Kumngern, T. Kulej, and D. Biolek, "0.3-volt rail-to-rail DDTA and its application in a universal filter and quadrature oscillator," *Sensors*, vol. 22, no. 7, p. 2655, Mar. 2022.

[18] T. Kulej, M. Kumngern, F. Khateb, and D. Arbet, "0.5 V versatile voltage- and transconductance-mode analog filter using differential difference transconductance amplifier," *Sensors*, vol. 23, no. 2, p. 688, Jan. 2023.

[19] P. Silapan, P. Choykhuntod, R. Kaewon, and W. Jaikla, "Duty-cycle electronically tunable triangular/square wave generator using LT1228 commercially available ICs for capacitive sensor interfacing," *Sensors*, vol. 22, no. 13, p. 4922, Jun. 2022.

[20] H. Alpaslan and E. Yuce, "DVCC+ based multifunction and universal filters with the high input impedance features," *Anal. Integr. Circuits Signal Process.*, vol. 103, no. 2, pp. 325–335, May 2020.

[21] F. Khateb, M. Kumngern, T. Kulej, and D. Biolek, "0.5 V differential difference transconductance amplifier and its application in voltage-mode universal filter," *IEEE Access*, vol. 10, pp. 43209–43220, 2022.

[22] N. A. Shan and M. A. Malik, "New high input impedance voltage-mode lowpass, bandpass and highpass filter using current feedback amplifiers," *J. Circuits Sys. Comput.*, vol. 14, no. 6, pp. 1037–1043, 2005.

[23] I. Mamatov, Y. Özçelep, and F. Kaçar, "Voltage differencing buffered amplifier based low power, high frequency and universal filters using 32 nm CNTFET technology," *Microelectron. J.*, vol. 107, Jan. 2021, Art. no. 104948.

[24] F. Kacar, A. Yesil, and A. Noori, "New CMOS realization of voltage differencing buffered amplifier and its biquad filter applications," *Radioengineering*, vol. 21, no. 1, pp. 333–339, Apr. 2012.

[25] J. Pimpol, N. Roongmuanpha, and W. Tangsrirat, "Low-output-impedance electronically adjustable universal filter using voltage differencing buffered amplifiers," in *Proc. 8th Int. Conf. Informat., Environ., Energy Appl. (IEEA)*. New York, NY, USA: Association for Computing Machinery, Mar. 2019, pp. 200–203.

[26] N. Roongmuanpha, T. Pukkalanun, and W. Tangsrirat, "Practical realization of electronically adjustable universal filter using commercially available IC-based VDBA," *Engineering Review*, vol. 41, no. 3, pp. 73–85, Sep. 2021.

[27] N. A. Shan and M. A. Malik, "High input impedance voltage-mode lowpass, bandpass, highpass and notch filter using current feedback amplifiers," *Indian J. Eng. Mater. Sci.*, vol. 12, pp. 278–280, Nov. 2005.

[28] S.-F. Wang, H.-P. Chen, Y. Ku, and P.-Y. Chen, "A CFOA-based voltage-mode multifunction biquadratic filter and a quadrature oscillator using the CFOA-based biquadratic filter," *Appl. Sci.*, vol. 9, no. 11, p. 2304, Jun. 2019.

[29] S.-F. Wang, H.-P. Chen, Y. Ku, and M.-X. Zhong, "Voltage-mode multifunction biquad filter and its application as fully-uncoupled quadrature oscillator based on current-feedback operational amplifiers," *Sensors*, vol. 20, no. 22, p. 6681, Nov. 2020.

[30] S.-F. Wang, H.-P. Chen, Y. Ku, and M.-X. Zhong, "Analytical synthesis of high-pass, band-pass and low-pass biquadratic filters and its quadrature oscillator application using current-feedback operational amplifiers," *IEEE Access*, vol. 9, pp. 13330–13343, 2021.

[31] S.-F. Wang, H.-P. Chen, Y. Ku, and Y.-F. Li, "High-input impedance voltage-mode multifunction filter," *Appl. Sci.*, vol. 11, no. 1, p. 387, Jan. 2021.

[32] D. R. Bhaskar, A. Raj, and R. Senani, "Three new CFOA-based SIMO-type universal active filter configurations with unrivalled features," *AEU Int. J. Electron. Commun.*, vol. 153, Aug. 2022, Art. no. 154285.

[33] M. Kumngern, P. Suksaibul, F. Khateb, and T. Kulej, "Electronically tunable universal filter and quadrature oscillator using low-voltage differential difference transconductance amplifiers," *IEEE Access*, vol. 10, pp. 68965–68980, 2022.

[34] S. Tuntrakool, M. Kumngern, R. Sotner, N. Herencsar, P. Suwanjan, and W. Jaikla, "High input impedance voltage-mode universal filter and its modification as quadrature oscillator using VDDDAs," *Indian J. Pure Appl. Phys.*, vol. 55, no. 5, pp. 324–332, May 2017.

[35] W. Jaikla, D. Biolek, S. Siripongdee, and J. Bajer, "High input impedance voltage-mode biquad filter using VD-DIBAs," *Radioengineering*, vol. 23, no. 3, pp. 914–921, Sep. 2014.

[36] W. Jaikla, S. Siripongdee, F. Khateb, R. Sotner, P. Silapan, P. Suwanjan, and A. Chaichana, "Synthesis of biquad filters using two VD-DIBAs with independent control of quality factor and natural frequency," *AEU Int. J. Electron. Commun.*, vol. 132, Apr. 2021, Art. no. 153601.

[37] S.-F. Wang, H.-P. Chen, Y. Ku, and C.-M. Yang, "Independently tunable voltage-mode OTA-C biquadratic filter with five inputs and three outputs and its fully-uncoupled quadrature sinusoidal oscillator application," *AEU Int. J. Electron. Commun.*, vol. 110, Oct. 2019, Art. no. 152822.

[38] S. F. Wang, H. P. Chen, Y. Ku, and Y. C. Lin, "Versatile tunable voltage-mode biquadratic filter and its application in quadrature oscillator," *Sensors*, vol. 19, no. 10, p. 2349, May 2019.

[39] S.-F. Wang, H.-P. Chen, Y. Ku, and C.-L. Lee, "Versatile voltage-mode biquadratic filter and quadrature oscillator using four OTAs and two grounded capacitors," *Electronics*, vol. 9, no. 9, p. 1493, Sep. 2020.

[40] N. Onanong, P. Supavarasuwat, D. Angamnuaysiri, S. Siripongdee, A. Chaichana, W. Jaikla, and P. Suwanjan, "Design of electronically controllable multifunction active filter with amplitude controllability using two commercially available ICs," *J. Electr. Comput. Eng.*, vol. 2022, pp. 1–11, Aug. 2022.

[41] S.-F. Wang, H.-P. Chen, Y. Ku, and W.-Y. Chen, "Isomorphic circuits of independent amplitude tunable voltage-mode bandpass filters and quadrature sinusoidal oscillators," *Appl. Sci.*, vol. 11, no. 16, p. 7431, Aug. 2021.

[42] M. P. P. Wai, P. Suwanjan, W. Jaikla, and A. Chaichana, "Electronically and orthogonally tunable SITO voltage-mode multifunction biquad filter using LT1228s," *Elektronika ir Elektrotechnika*, vol. 27, no. 5, pp. 11–17, Oct. 2021.

[43] H.-P. Chen, S.-J. Chen, and C.-Y. Chang, "Synthesis of high-input impedance electronically tunable voltage-mode second-order low-pass, band-pass, and high-pass filters based on LT1228 integrated circuits," *Sensors*, vol. 22, no. 23, p. 9379, Dec. 2022.

[44] Linear Technology Corporation. (2012) *LT1228—100 MHz Current Feedback Amplifier With DC Gain Control Linear Technology Corporation Version Number D*. Accessed: 12 May 2019. [Online]. Available: http://www.linear.com/product/LT1228

[45] Y. Sun and J. K. Fidler, "Versatile active biquad based on second-generation current conveyors," *Int. J. Electron.*, vol. 76, no. 1, pp. 91–98, Jan. 1994.

[46] S. Maheshwari, S. V. Singh, and D. S. Chauhan, "Electronically tunable low-voltage mixed-mode universal biquad filter," *IET Circuits, Devices Syst.*, vol. 5, no. 3, pp. 149–158, May 2011.

[47] S. Boctor, "A novel second-order canonical RC-active realization of high-pass notch filter," *IEEE Trans. Circuits Syst.*, vol. CS-22, no. 5, pp. 397–404, May 1975.

[48] S. Boctor, "Single amplifier functionally tunable low-pass-notch filter," *IEEE Trans. Circuits Syst.*, vol. CS-22, no. 11, pp. 875–881, Nov. 1975.

[49] A. Kircay and U. Cam, "Differential type class-AB second-order log-domain notch filter," *IEEE Trans. Circuits Syst. I, Reg. Papers*, vol. 55, no. 5, pp. 1203–1212, Jun. 2008.

[50] S.-Y. Lee, C.-P. Wang, and Y.-S. Chu, "Low-voltage OTA–C filter with an area- and power-efficient OTA for biosignal sensor applications," *IEEE Trans. Biomed. Circuits Syst.*, vol. 13, no. 1, pp. 56–67, Feb. 2019.

[51] R. Arya and J. P. Oliveira, "Gm-C biquad filter for low signal sensor applications," in *Proc. MIXDES 23rd Int. Conf. Mixed Design Integr. Circuits Syst.*, Jun. 2016, pp. 207–210.

[52] W. Kamp, R. Kunemund, H. Soldner, and R. Hofer, "Programmable 2D linear filter for video applications," *IEEE J. Solid-State Circuits*, vol. 25, no. 3, pp. 735–740, Jun. 1990.

[53] S.-S. Lee and C. A. Laber, "A BiCMOS continuous-time filter for video signal processing applications," *IEEE J. Solid-State Circuits*, vol. 33, no. 9, pp. 1373–1382, Sep. 1998.

[54] Z. Y. Chang, D. Haspeslagh, J. Boxho, and D. Macq, "A highly linear CMOS Gm-C bandpass filter for video applications," in *Proc. Custom Integr. Circuits Conf.*, May 1996, pp. 89–92.

[55] M. A. Ibrahim, S. Minaei, and H Kuntman, "A 22.5 MHz current-mode KHN-biquad using differential voltage current conveyor and grounded passive elements," *AEU Int. J. Electron. Commun.*, vol. 59, no. 5, pp. 311–318, Jul. 2005.

[56] F. A. P. Bariqui, A. Petraglia, and E. Rapoport, "IC design of an analog tunable crossover network," in *Proc. IEEE Int. Symp. Circuits Syst.*, vol. 2, May 2005, pp. 1012–1015.

[57] E. Rapoport, F. A. P. Baruqui, and A. Petraglia, "Tunable analog loudspeaker crossover network," in *Proc. IEEE Int. Symp. Circuits Syst. (ISCAS)*, May 2003, pp. 477–480.

[58] V. Chutchavong, T. Muantoei, and K. Janchitrapongvej, "A new method for design of the three-way crossover networks," in *Proc. 4th Joint Int. Conf. Inf. Commun. Technol., Electron. Electr. Eng. (JICTEE)*, Mar. 2014, pp. 1–5.

[59] X. Qian, Y. P. Xu, and X. Li, "A CMOS continuous-time low-pass notch filter for EEG systems," *Analog Integr. Circuits Signal Process.*, vol. 44, no. 3, pp. 231–238, Sep. 2005.

[60] T. Unuk and E. Yuce, "A mixed-mode filter with DVCCs and grounded passive components only," *AEU Int. J. Electron. Commun.*, vol. 144, Feb. 2022, Art. no. 154063.

[61] N. Herencsar, R. Sotner, J. Koton, J. Misurec, and K. Vrba, "New compact VM four-phase oscillator employing only single Z-copy VDTA and all grounded passive elements," *Electron. Electr. Eng.*, vol. 19, no. 10, pp. 87–90, Dec. 2013.

[62] S.-F. Wang and H.-P. Chen, "New voltage-mode sinusoidal oscillators using VDIBAs," *J. Circuits, Syst. Comput.*, vol. 29, no. 4, Mar. 2020, Art. no. 2050052.

[63] D. Biolek and V. Biolkova, "First-order voltage-mode all-pass filter employing one active element and one grounded capacitor," *Anal. Integr. Circuits Signal Process.*, vol. 65, no. 1, pp. 123–129, Oct. 2010.

[64] N. Herencsar, S. Minaei, J. Koton, E. Yuce, and K. Vrba, "New resistorless and electronically tunable realization of dual-output VM all-pass filter using VDIBA," *Analog Integr. Circuits Signal Process.*, vol. 74, no. 1, pp. 141–154, Jan. 2013.

[65] V. Biolkova, J. Bajer, and D. Biolek, "Four-phase oscillators employing two active elements," *Radioengineering*, vol. 20, no. 1, pp. 334–339, 2011.

[66] D. Singh and S. K. Paul, "Realization of current mode universal shadow filter," *AEU Int. J. Electron. Commun.*, vol. 117, Apr. 2020, Art. no. 153088.

[67] H.-P. Chen, Y.-S. Hwang, and Y.-T. Ku, "A new resistorless and electronic tunable third-order quadrature oscillator with current and voltage outputs," *IETE Tech. Rev.*, vol. 35, no. 4, pp. 426–438, May 2017.

[68] M. Faseehuddin, N. Herencsar, S. Shireen, W. Tangsrirat, and S. H. Md Ali, "Voltage differencing buffered amplifier-based novel truly mixed-mode biquadratic universal filter with versatile input/output features," *Appl. Sci.*, vol. 12, no. 3, p. 1229, Jan. 2022.

[69] M. Kumngern, P. Lamun, and K. Dejhan, "Current-mode quadrature oscillator using current differencing transconductance amplifiers," *Int. J. Electron.*, vol. 99, no. 7, pp. 971–986, Feb. 2012.

[70] M. Kumngern, P. Suksaibul, F. Khateb, and T. Kulej, "1.2 V differential difference transconductance amplifier and its application in mixed-mode universal filter," *Sensors*, vol. 22, no. 9, p. 3535, May 2022.

[71] N. Roongmuanpha, W. Tangsrirat, and T. Pukkalanun, "Single VDGA-based mixed-mode universal filter and dual-mode quadrature oscillator," *Sensors*, vol. 22, no. 14, p. 5303, Jul. 2022.

[72] W. Jaikla, F. Khateb, T. Kulej, and K. Pitaksuttayaprot, "Universal filter based on compact CMOS structure of VDDDA," *Sensors*, vol. 21, no. 5, p. 1683, Mar. 2021.

[73] P. Huaihongthong, A. Chaichana, P. Suwanjan, S. Siripongdee, W. Sunthonkanokpong, P. Supavarasuwat, W. Jaikla, and F. Khateb, "Single-input multiple-output voltage-mode shadow filter based on VDDDAs," *AEU Int. J. Electron. Commun.*, vol. 103, pp. 13–23, May 2019.

[74] P. Supavarasuwat, M. Kumngern, S. Sangyaem, W. Jaikla, and F. Khateb, "Cascadable independently and electronically tunable voltage-mode universal filter with grounded passive components," *AEU Int. J. Electron. Commun.*, vol. 84, pp. 290–299, Feb. 2018.

[75] W. Ninsraku, D. Biolek, W. Jaikla, S. Siripongdee, and P. Suwanjan, "Electronically controlled high input and low output impedance voltage mode multifunction filter with grounded capacitors," *AEU Int. J. Electron. Commun.*, vol. 68, no. 12, pp. 1239–1246, Dec. 2014.

[76] W. Jaikla, U. Buakhong, S. Siripongdee, F. Khateb, R. Sotner, P. Silapan, P. Suwanjan, and A. Chaichana, "Single commercially available IC-based electronically controllable voltage-mode first-order multifunction filter with complete standard functions and low output impedance," *Sensors*, vol. 21, no. 21, p. 7376, Nov. 2021.

[77] N. Roongmuanpha, M. Faseehuddin, N. Herencsar, and W. Tangsrirat, "Tunable mixed-mode voltage differencing buffered amplifier-based universal filter with independently high-Q factor controllability," *Appl. Sci.*, vol. 11, no. 20, p. 9606, Oct. 2021.

**SAN-FU WANG** was born in Changhua, Taiwan, in 1976. He received the M.S. and Ph.D. degrees from the Department of Electronic Engineering, Institute of Computer and Communication, National Taipei University of Technology, Taipei, Taiwan, in 2003 and 2010, respectively. He is currently an Associate Professor with the Department of Electronic Engineering, National Chin-Yi University of Technology, Taichung, Taiwan. His research interests include mixed-signal integrated circuits and analog signal processing.

**CHIH-YANG CHANG** was born in Taiwan, in 1998. He received the B.S. degree in electronic engineering from the Ming Chi University of Technology, New Taipei, Taiwan, in 2021, where he is currently pursuing the M.S. degree in electronic engineering. His research interests include analog circuits design, printed circuit board design, and analytical verification using OrCAD PSpice and MATLAB software.

**SHIH-JUN CHEN** received the B.S. degree in electronic engineering from the Ming Chi University of Technology, New Taipei, Taiwan, in 2021, where he is currently pursuing the M.S. degree in electronic engineering. His research interests include analog integrated circuit design and plastic circuit board design including filter and oscillator, which assists verifying the ability of integrated circuit circuits. He is also good in simulating circuits using OrCAD PSpice and MATLAB software.

**HUA-PIN CHEN** received the M.S. and Ph.D. degrees from Chung Yuan Christian University, Taoyuan, Taiwan, in 2001 and 2005, respectively. In August 2009, he joined the Department of Electronic Engineering, Ming Chi University of Technology, New Taipei, Taiwan, as an Associate Professor, where he is currently a Professor. His research interests include circuits and systems, analog and digital electronics, active filter/oscillator design current-mode integrated circuits, and current-mode signal processing.

**YU-HSI CHEN** was born in Taiwan, in 2003. He is currently pursuing the B.S. degree in electrical engineering with National Formosa University, Huwei, Yunlin, Taiwan. His research interests include integrated circuit design and verification, chip layout, pre- and post-layout simulations, and analytical verification in Virtuoso and Hspice.

· · ·